
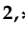







## Article

# Anodizing of AA2024 Aluminum–Copper Alloy in Citric-Sulfuric Acid Solution: Effect of Current Density on Corrosion Resistance

Jose Cabral-Miramontes <sup>1</sup>, Noe Cabral-Miramontes <sup>1</sup>, Demetrio Nieves-Mendoza <sup>2,\*</sup>, Maria Lara-Banda <sup>1,\*</sup>, Erick Maldonado-Bandala <sup>2</sup>, Javier Olguín-Coca <sup>3</sup>, Luis Daimir Lopez-Leon <sup>3</sup>, Francisco Estupiñan-Lopez <sup>1</sup>, F. Almeraya Calderon <sup>1,\*</sup> and Citlalli Gaona Tiburcio <sup>1</sup>

- <sup>1</sup> Universidad Autónoma de Nuevo León, Centro de Investigación e Innovación en Ingeniería Aeronáutica (CIIIA), FIME, San Nicolás de los Garza 66455, Mexico; jose.cabralmr@uanl.edu.mx (J.C.-M.); 18040386@itdurango.edu.mx (N.C.-M.); francisco.estupinanlp@uanl.edu.mx (F.E.-L.); citlalli.gaonatbr@uanl.edu.mx (C.G.T.)
- <sup>2</sup> Facultad de Ingeniería Civil, Universidad Veracruzana, Xalapa 91000, Mexico; erimaldonado@uv.mx
- <sup>3</sup> Área Académica de Ingeniería y Arquitectura, Universidad Autónoma del Estado de Hidalgo, Carretera Pachuca-Tulancingo Km. 4.5., Pachuca 42082, Mexico; olguinc@uaeh.edu.mx (J.O.-C.); luis\_lopez@uaeh.edu.mx (L.D.L.-L.)
- \* Correspondence: dnieves@uv.mx (D.N.-M.); maria.laraba@uanl.edu.mx (M.L.-B.); facundo.almerayaacd@uanl.edu.mx (F.A.C.)



**Citation:** Cabral-Miramontes, J.; Cabral-Miramontes, N.; Nieves-Mendoza, D.; Lara-Banda, M.; Maldonado-Bandala, E.; Olguín-Coca, J.; Lopez-Leon, L.D.; Estupiñan-Lopez, F.; Calderon, F.A.; Gaona Tiburcio, C. Anodizing of AA2024 Aluminum–Copper Alloy in Citric-Sulfuric Acid Solution: Effect of Current Density on Corrosion Resistance. *Coatings* **2024**, *14*, 816. <https://doi.org/10.3390/coatings14070816>

Academic Editors: Jianwei Dai, Mohammad Reza Loghman-Estarki and Lei Guo

Received: 24 May 2024  
Revised: 24 June 2024  
Accepted: 27 June 2024  
Published: 30 June 2024



**Copyright:** © 2024 by the authors. Licensee MDPI, Basel, Switzerland. This article is an open access article distributed under the terms and conditions of the Creative Commons Attribution (CC BY) license (<https://creativecommons.org/licenses/by/4.0/>).

**Abstract:** Al–Cu alloys are widely used as a structural material in the manufacture of commercial aircraft due to their high mechanical properties such as hardness, strength, low density, and tolerance to fatigue damage and corrosion. One of the main problems of these Al–Cu alloy systems is their low corrosion resistance. The purpose of this study is to analyze the influence of anodizing parameters on aluminum–copper alloy (AA 2024) using a bath of citric-sulfuric acid with different anodizing current densities on the thickness, microhardness, and corrosion resistance of the anodized layer. Hard anodizing is performed on AA 2024 Al–Cu alloy in mixtures of solutions composed of citric and sulfuric acid at different concentrations for 60 min and using current densities (*i*) of 0.03, 0.045, and 0.06 A/cm<sup>2</sup>. Scanning electron microscopy (SEM) was used to analyze the surface morphology and thickness of the anodized layer. The mechanical properties of the hard anodized material are evaluated using the Vickers hardness test. The electrochemical techniques use cyclic potentiodynamic polarization curves (CPPC) according to ASTM-G6 and electrochemical impedance spectroscopy (EIS) according to ASTM-G61 and ASTM-G106, respectively, in the electrolyte of NaCl at 3.5 wt. % as a simulation of the marine atmosphere. The results indicate that corrosion resistance anodizing in citric-sulfuric acid solutions with a current density of 0.06 A/cm<sup>2</sup> is the best with a corrosion current density (*j*<sub>corr</sub>) of 1.29 × 10<sup>−8</sup> A/cm<sup>2</sup>. It is possible to produce hard anodizing with citric and sulfuric acid solutions that exhibit mechanical properties and corrosion resistance similar or superior to conventional sulfuric acid anodizing.

**Keywords:** aerospace alloy; corrosion; anodizing; electrochemistry

## 1. Introduction

The aeronautical industry has an important role in developing and applying new materials and technologies because damage tolerance is especially low in this industry. For this reason, materials should present excellent properties for service conditions. Constant optimization processes should be carried out to increase mechanical, fatigue, corrosion, and oxidation resistance, which should be certified and satisfy security standards.

Aluminum (Al) is the most important of the non-ferrous metals, offering favorable mechanical characteristics, notably good machinability, high ductility, and low density (2.71 g/cm<sup>3</sup>) [1]. Therefore, it is combined with other elements to form alloys, obtaining

improvements in its mechanical properties, thus offering the industry better mechanical strength and corrosion resistance [2,3]. The 2XXX (Al–Cu) series alloys offer excellent mechanical properties/weight ratios and low cost. Because of this, they are frequently used for various structural components in the aerospace sector, such as for manufacturing fatigue-resistant, damage-tolerant structures requiring high specific strength [4–8]. However, this alloy has a high copper percentage, which causes poor anodic coating quality and corrosion problems [9,10]. These corrosion problems are mainly due to the formation of galvanic couples between the alloy's matrix and intermetallic phases, which are mainly responsible for improving the mechanical properties. When aluminum encounters oxygen in the air, it naturally forms a coating of aluminum oxide ( $\text{Al}_2\text{O}_3$ ), whose thickness varies between  $3 \times 10^{-3}$  and  $0.01 \mu\text{m}$ , which makes it a corrosion-tolerant metal [1]. Aluminum alloys are best protected from corrosive environments, such as atmospheric and/or marine environments, by coating their surface with thick oxide layers. Anodizing is a commercial procedure used to give aluminum alloys greater characteristics and increased resistance to corrosion. It is the most popular and economical option [3,11]. Many industries use anodized aluminum, including aerospace, electronics, maritime, architecture, and aeronautics. The application of this method extends to cooling procedures for aluminum mold thermal protection [12,13].

Anodizing is an electrochemical process in which an anodic film of alumina ( $\text{Al}_2\text{O}_3$ ) is grown in a controlled manner with constant current or potential on aluminum in an electrochemical cell containing a neutral or acid electrolyte [1]. During the process, the aluminum part acts as an anode, and the cathodes used are also made of aluminum or materials such as graphite, stainless steel, and lead [14]. The formed anodic film's quality and thickness can be controlled by different factors such as anodizing current density, acid concentration, composition, electrolyte temperature, and anodizing time [15]. In general, one of the most crucial factors influencing the microstructure and properties of the coating is the current density [16]. During this process, an anodic oxide layer is formed on the aluminum alloy surface, which affects the mechanical characteristics, chemical makeup, and morphology [17,18]. One of the most significant anodizing techniques for aluminum–copper alloy (AA 2024) in aircraft applications is hard anodizing, also known as type III anodizing. Hard anodizing is widely used in industrial applications because of increased mechanical properties, where a denser coating is created with a film thickness between 20 and  $120 \mu\text{m}$  [17,19–21], and improved corrosion resistance [22]. Some benefits of the type III hard anodizing process include increased abrasion, corrosion and wear resistance, hardness, improved adhesive bonding and lubrication, and improved decorative appearance [14,17]. Unfortunately, chromic and sulfuric acid are applied for most type III hard coatings, which are of high risk to human health [23,24]. Numerous studies showed that the anodic layer thickness increases with increasing acid content [25].

Acidic electrolytes are known to create porous oxide films because they have low acid dissociation constants ( $\text{pK}_a$ ). These electrolytes fall into three categories: inorganic, organic carboxylic, and organic cyclic oxocarbonic acids. One of the greatest substitutes for inorganic acids (chromic, phosphoric, and sulfuric acid) are organic carboxylic acids such as oxalic, malonic, and citric and other less common ones such as tartaric, glycolic, tartaric, and formic. However, the latter involves the application of high voltages (150 to 450 V) to carry out the anodizing process [26]. Table 1 shows the  $\text{pK}_a$  values of the inorganic acids and organic carboxylic acids most used as additives in anodizing processes and found in some published works. One of the most typical mechanisms of additive reactions is the creation of aluminum complexes with organic carboxylic molecules. In this particular case, the anodic coatings incorporate insoluble metal soaps, which are produced through the easy formation of complexes between hard-ion carboxylates and trivalent aluminum cations. Since the  $\text{pK}_a$  of carboxylic acids is greater than the pH of the sulfuric acid baths, the molecules will likely protonate and turn neutral in solution, losing their propensity to migrate toward the anode. On the oxide surface, the complexed additives create a thin layer that shields the metal, and, in this way, citric acid improves the properties of the

anodic coating formed [27]. The citric acid ( $C_6H_8O_7$ ), an alternative for the substitution of sulfuric acid, is abundant and does not generate environmental hazards. This enhances the anodic film characteristics. In addition, this acid does not need higher concentrations to provide better protection and generally performs great on aluminum alloys [28–30].

**Table 1.**  $pK_a$  and works published of inorganic acids and with additions of organic carboxylic acids.

Acid	Formula	$pK_a$	Work Published and Year	Ref
Chromic	$H_2CrO_4$	−0.98	Stepniowski, et al., 2012	[31]
			Stepniowski, et al., 2014	[32]
Phosphoric	$H_3PO_4$	2.2	Le Coz, et al., 2010	[33]
			Masuda, et al., 1998	[34]
Sulfuric	$H_2SO_4$	−3.0	Guthrie P.J. 1976	[35]
			Poznyak, et al., 2021	[36]
			De Graeve, et al., 2003	[37]
Citric	$C_6H_8O_7$	3.09	Martell, A.E, et al., 1976	[30]
			Cabral, et al., 2020	[38]
			Poznyak, et al., 2020	[39]
			Cabral, et al., 2022	[40]
Oxalic	$C_2H_2O_4$	1.23	Sulka, et al., 2010	[41]
			Stepniowski, et al., 2013	[42]
Malonic	$C_3H_4O_4$	2.83	Ren, et al., 2012	[43]
			Vrublevsky, et al., 2009	[44]
Tartaric	$C_4H_6O_6$	2.99	Chu, et al., 2006	[45]
			Vrublevsky, et al., 2014	[46]

This work aims to study an electrochemical treatment (anodizing) using citric and sulfuric acid to obtain type III hard anodizing on Al–Cu alloy and determine the behavior of the protective layer with increasing current density ( $i = 0.03, 0.045, \text{ and } 0.06 \text{ A/cm}^2$ ). Scanning electron microscopy (SEM) was used to analyze the surface morphology and thickness of the anodized layer. The mechanical properties of the hard anodized material were evaluated using the Vickers hardness test. The electrochemical techniques used cyclic potentiodynamic polarization curves (CPPC) according to ASTM-G61-86 [47] and electrochemical impedance spectroscopy (EIS) according to ASTM-G106 [48], exposed to a 3.5 wt.% NaCl aqueous solution. Aircraft aluminum alloys are exposed to different atmospheres, such as marine and industrial (acid rain). The characterization using electrochemical techniques of aluminum alloys could find potential applications in the aeronautical industry, such as in fuselages and spars.

## 2. Materials and Methods

### 2.1. Material

A commercial alloy of Al–Cu 2024 alloy was used, which is widely used in constructing fuselages. While it only has a moderate yield strength, it has excellent resistance to fatigue crack growth and good fracture toughness. The form of a  $50 \pm 2.5 \text{ mm}$  diameter bar was used, and disks of  $5 \pm 0.25 \text{ mm}$  in thickness were cut as examples before being anodized. With the following nominal chemical composition by weight (wt.%) of 4.2 wt.% Cu, 0.48 wt.% Mn, 1.4 wt.% Mg, 0.5% wt.% Si, 0.5 wt.% Fe, 0.1% wt.% Cr, 0.25% wt.% Zn, 0.15% wt.% Ti and balance of Al. AA 2024 samples were polished following ASTM E3 and E407 standards [49,50] before the SiC papers of grades 180, 220, 320, 400, and 600 were anodized; this was followed by 10 min in ultrasonic cleaning in ethanol and air drying.

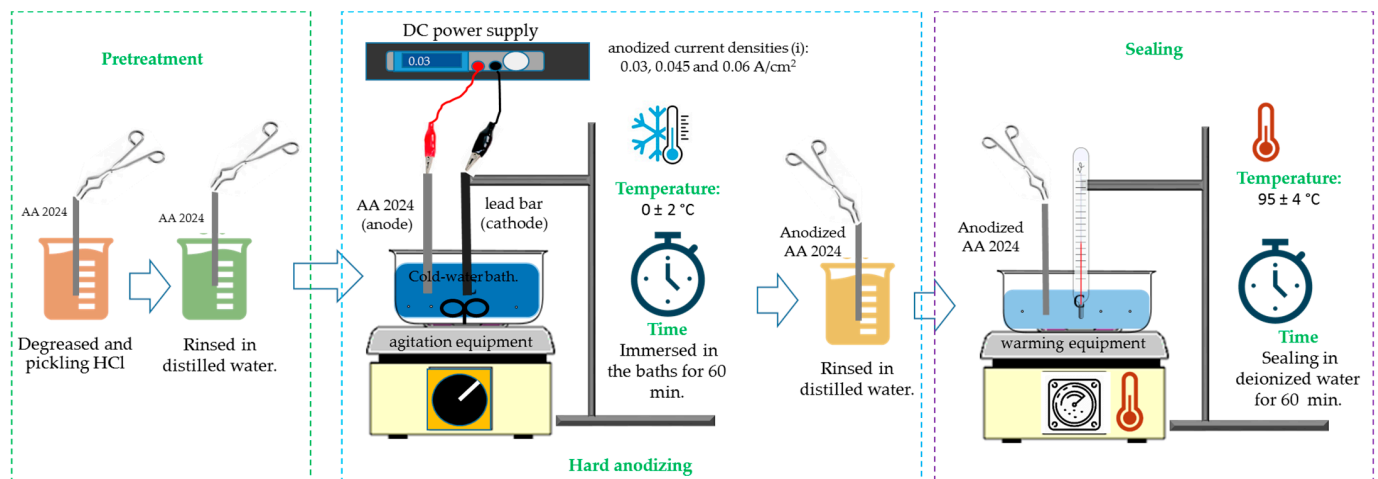
## 2.2. Electrochemical Treatment: Hard Anodizing

The anodizing treatment required five seconds of pickling in a 1:1 solution of HCl, followed by 3 rinses in deionized water to remove the remaining HCl solution from the samples. The following bath solutions were applied to anodize AA 2024: 1M citric acid concentration, a 1M sulfuric acid solution as a control, a solution consisting of a 1M citric acid concentration with 5 mL/Liter additions of sulfuric acid, and finally a solution composed of a 1M citric acid concentration with 10 mL/Liter additions of sulfuric acid. Four solutions produced type III hard anodizing of AA 2024 aluminum–copper alloys. A lead bar was used as the cathode. A DC power supply was used as a high-power current generator, model XLN30052-GL (Yorba Linda, CA, USA), four distinct electrolyte solutions and anodized current densities (i) of 0.03, 0.045, and 0.06 A/cm<sup>2</sup> were the parameters utilized in the anodizing process [51]. The anodization process was conducted for one hour at  $0 \pm 2$  °C in a cold-water bath while the solution was continuously stirred. In type III hard anodizing, temperature fluctuation is very important, so it must be controlled and kept as low as possible since excess electricity produces heat, which causes partial or total dissolution of the film [52]. After anodizing, the parts were rinsed in deionized water, and then a sealing process was applied, which consisted of immersion for one hour in deionized water at a temperature of  $95 \pm 4$  °C. The hot water sealing process increases corrosion resistance, reduces or eliminates porosity in the anodizing, reduces the deterioration phenomenon known as efflorescence (exposure of aluminum outdoors), and improves abrasion resistance [53,54]. The anodizing process parameters and sample nomenclature utilized in this work are presented in Table 2. Figure 1 shows the anodizing process used in this work.

**Table 2.** Anodizing treatment parameters and sample nomenclature.

Material	Anodizing				Sealing	Nomenclature
	Current Density (i), A/cm <sup>2</sup>	Time and Temperature	Solutions Concentration Citric Acid	Sulfuric Acid		
AA 2024	0.03	Time 1 h Temperature $0 \pm 2$ °C	1 M	-	Deionized water Temperature $95 \pm 4$ °C Time 1 h	0.03 A 1MC
			-	1M		0.03 A 1MS
			1 M	5 mL/L		0.03 A 1MC 5S
			1 M	10 mL/L		0.03A 1MC 10S
	0.045		1 M	-		0.045A 1MC
			-	1M		0.045A 1MS
			1 M	5 mL/L		0.045A 1MC 5S
			1 M	10 mL/L		0.045A 1MC 10S
	0.06		1 M	-		0.06A 1MC
			-	1 M		0.06A 1MS
			1 M	5 mL/L		0.06 A 1MC 5S
			1 M	10 mL/L		0.06 A 1MC 10S





**Figure 1.** Diagram of the anodizing treatment of Al–Cu 2024.

### 2.3. Microstructural Characterization

Scanning electron microscopy was utilized to examine the microstructure with Zeiss model Sigma 300 VP [Oberkochen, Baden-Wurtemberg, Germany] equipment to analyze the anodizing layer thickness (cross-section), obtaining an average of 5 measurements per image in the SEM software V 1.0, and surface morphology of the anodized specimens at a magnification of  $2000\times$ . Backscattered electrons (BSE) with beam energy of 20 kV, were used to observe the morphology, and energy dispersive X-ray spectroscopy (EDS) was used to determine the chemical composition of the cross sections and perform element mapping.

### 2.4. Vickers Hardness Test

The cross-section of the anodized specimen was measured with Vickers hardness using a microhardness tester [Wilson Tester 402 MVD, Lake Bluff, IL, USA]; fifteen readings per sample were obtained with a 0.05 gf load and a 15-s dwell period in accordance with ASTM E92 [55].

### 2.5. Electrochemical Measurements

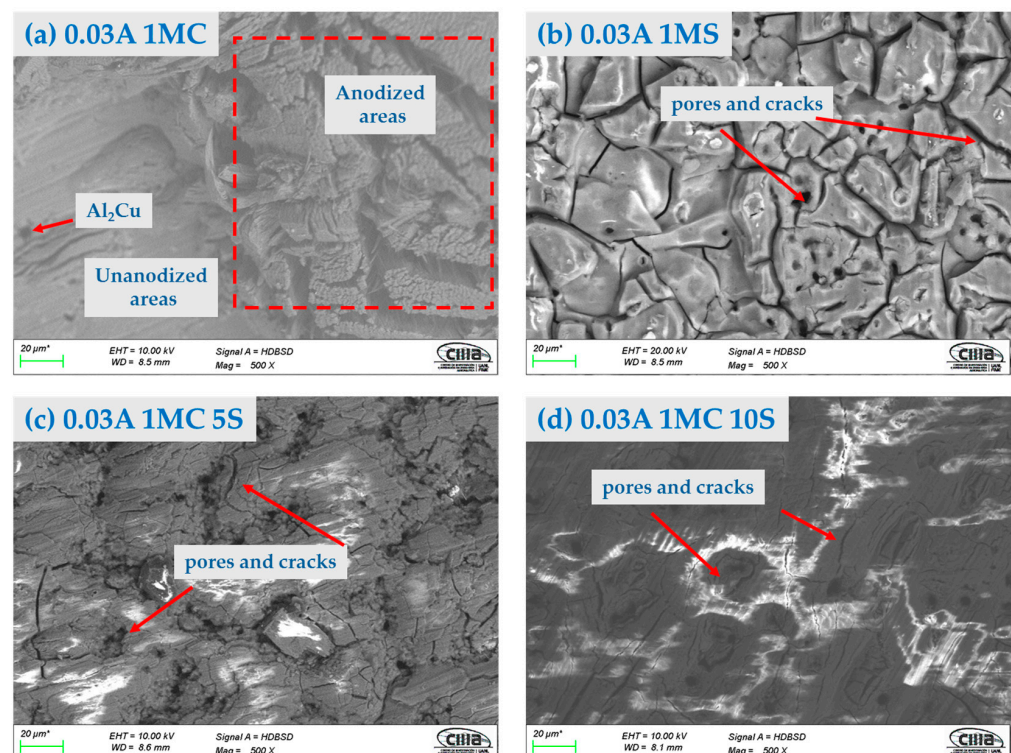
Electrochemical measurements were performed using a three-electrode cell. A saturated calomel reference electrode (SCE), a platinum counter electrode, and anodized samples were used as working electrodes. A potentiostat/galvanostat/ZRA Solartron 1287 A (Bognor Regis, UK) was used. All tests were performed by immersion in a 3.5 wt.% NaCl solution at room temperature and the tests were performed in duplicate. Cyclic potentiodynamic polarization curve testing (CPPC) was used to determine the corrosion resistance of the anodized parts in different solutions and at different current densities. The CPPC was performed with a potential sweep from  $-0.3$  to  $1.0$  V of OCP, with a scan rate of  $0.06$  V/min applied, and a complete polarization cycle according to ASTM G61-11 [47]. EIS has measured a frequency range of 0.01 to 100,000 Hz, obtaining 35 points per decade, and using a 10 mV RMS amplitude by the ASTM G106-15 standard [48]. The spectra of EIS were analyzed in terms of an equivalent circuit using “Zview-4” software (<https://www.scribner.com/software/68-general-electrochemistr376-zview-for-windows/>) (Scribner Associates, Inc. por Berek Johnson, Southern Pines, NC, USA).

### 3. Results and Discussion

#### 3.1. Microstructural Characterization by SEM

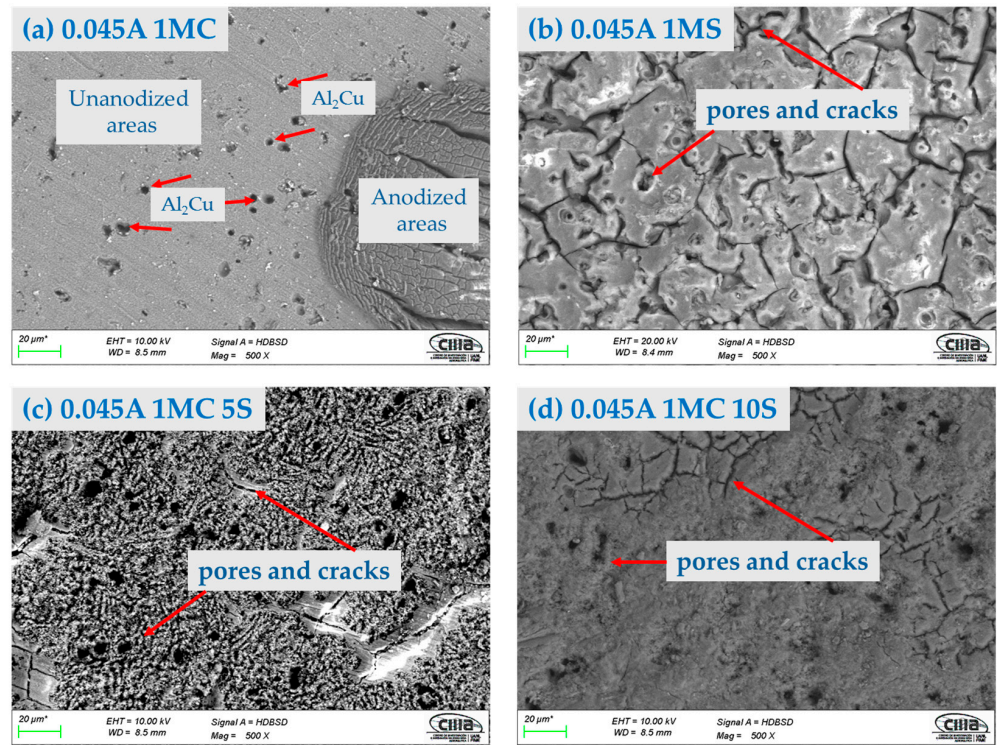
##### 3.1.1. Surface Morphology

Figures 2–4 show the surface morphology obtained by SEM of the anodized samples with different current densities of 0.03, 0.045, and 0.06 A/cm<sup>2</sup> in the bath solutions. All the anodized samples with a current density of 0.03 A/cm<sup>2</sup> presented surface cracking and porosity in the coating. This same behavior was present in the samples with current densities of 0.045 and 0.06 A/cm<sup>2</sup>, irrespective of the bath solution used in the anodizing process. The presence of areas without anodizing coating can be observed in the samples anodized in 1M citric acid solution. These areas are in Figures 2a, 3a, and 4a,c. These images also show the intermetallic compounds of this alloy formed by Al, Cu, Mg, and Fe. This behavior may be because the fully manufactured citric acid solution is not able to form the necessary compounds to grow the oxide layer in the anodizing process, since it has been reported that in anodizing in baths formed by organic acids, long-term voltages higher than 350 V and temperatures below 0 °C are necessary to grow non-homogeneous anodic layers [56,57]. This same behavior was present in sample 0.06 A1MC 5 S. The samples anodized in 1M H<sub>2</sub>SO<sub>4</sub> solution with (i) of 0.03, 0.045, and 0.06 A/cm<sup>2</sup> (Figures 2b, 3b, and 4b) presented the same surface morphology called “dry mud or soil”, which has been described by other authors as Soffritti et al. and Guezmil et al. [58,59]. The samples anodized in citric and sulfuric acid mixtures with different current densities showed surface cracking and porosity; however, in most cases, the coating is continuous over the entire surface. This type of surface morphology has been observed in anodizing produced with tertiary and boric acid on AA1050 (pure aluminum) and 2024 T3 (aluminum–copper alloy with thermal treatment, cold worked, and aged naturally) alloys [60,61].

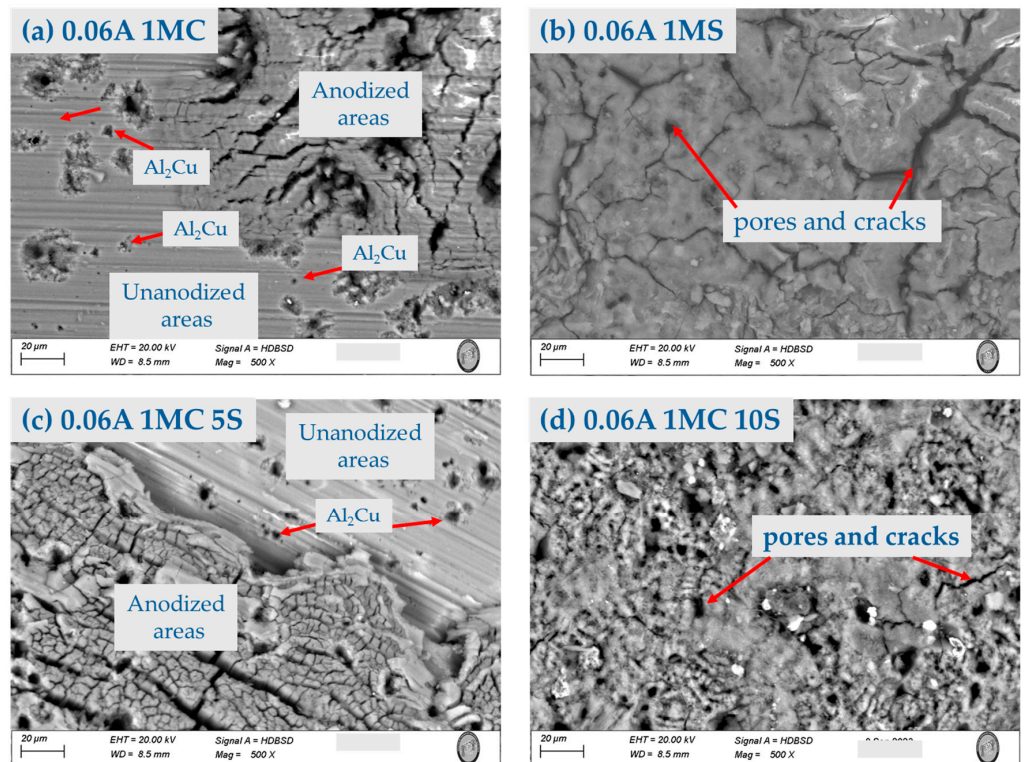


**Figure 2.** Surface morphology by SEM-BSE of the AA2024 anodized at 0.03 A/cm<sup>2</sup> in different bath solutions: (a) 1MC; (b) 1MS; (c) 1MC 5S; and (d) 1MC 10S.





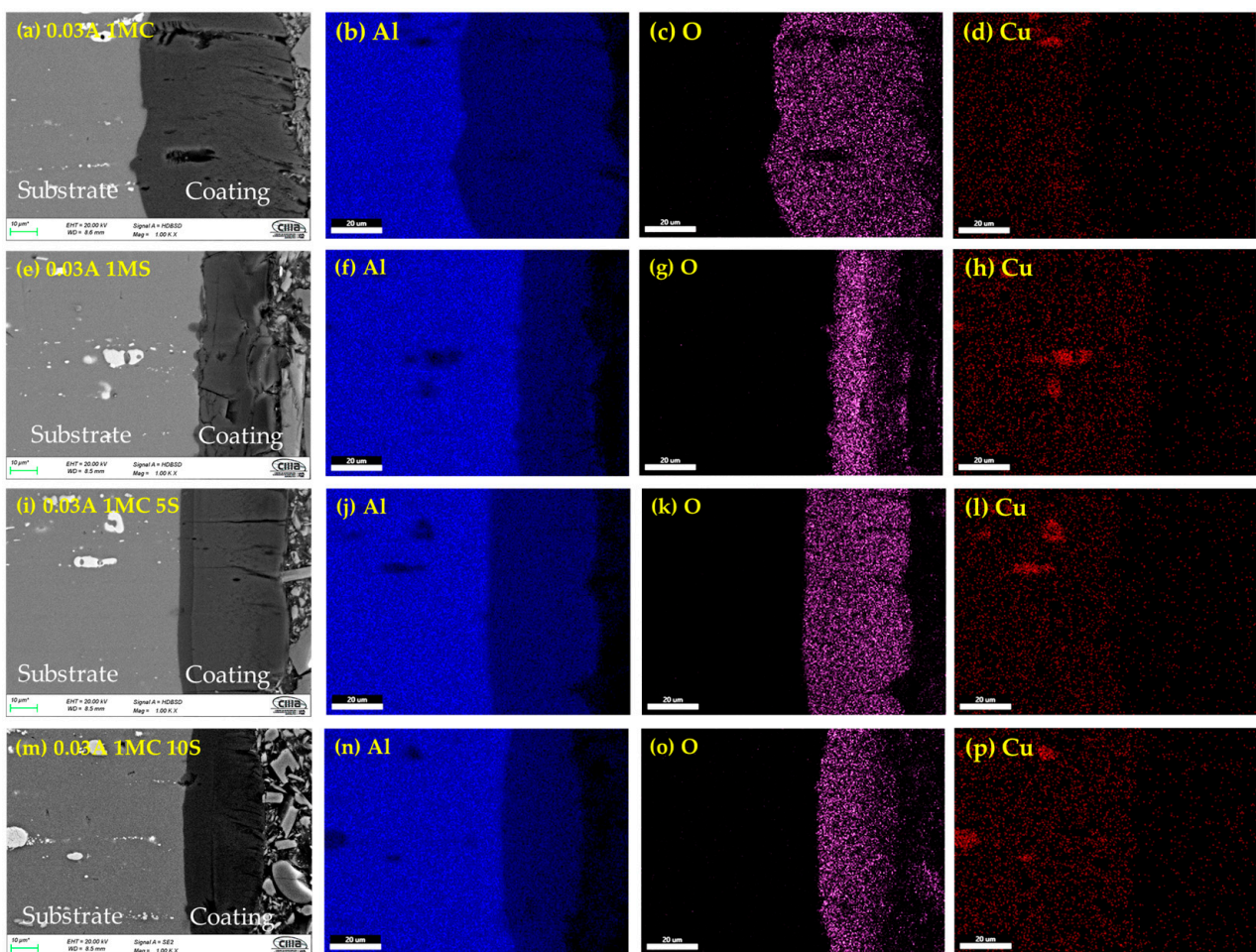
**Figure 3.** Surface morphology by SEM-BSE of the AA2024 anodized at 0.045 A/cm<sup>2</sup> in different baths solutions: (a) 1MC; (b) 1MS; (c) 1MC 5S; and (d) 1MC 10S.



**Figure 4.** Surface morphology by SEM-BSE of the AA2024 anodized at 0.06 A/cm<sup>2</sup> in different baths solutions: (a) 1MC; (b) 1MS; (c) 1MC 5S; and (d) 1MC 10S.

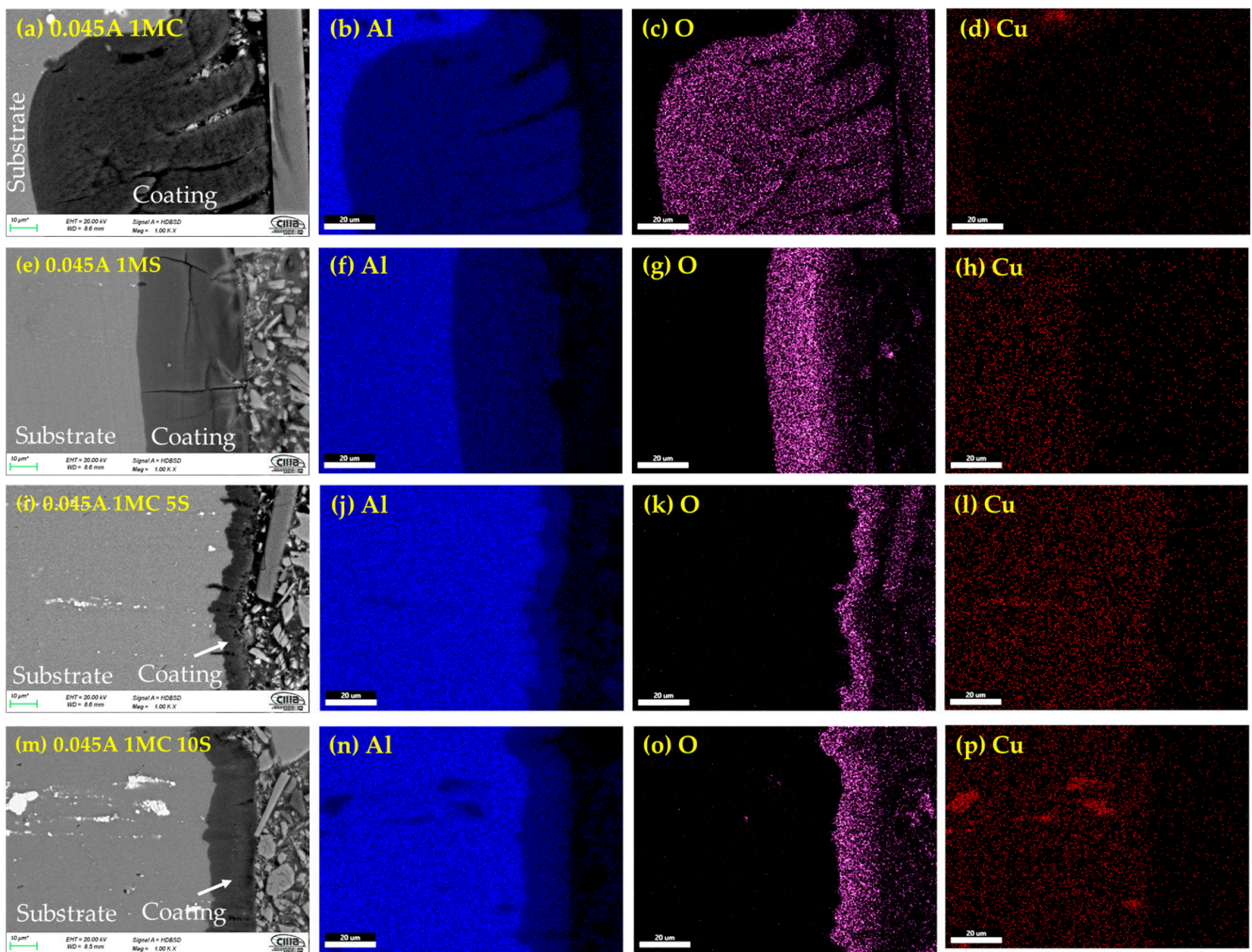
### 3.1.2. Morphology of Cross Section by SEM

The cross-sectional micrographs obtained using SEM and the chemical composition mapping obtained by EDS of the anodized AA 2024 alloy under various conditions are shown in Figures 5–7. Figure 5a,e,i,m clearly show the anodized coating layer obtained in the different solutions. Porosity and cracks in these coatings can occasionally extend from the surface of the coating into the base material. This same cracking behavior can also be observed in the samples anodized with 0.045 and 0.06 A/cm<sup>2</sup>, extending to the base metal from the coatings surface (Figures 6 and 7). The second column represents the aluminum content in the samples, and the third column indicates high oxygen concentrations in all cases, which correspond to the aluminum oxide layer (alumina Al<sub>2</sub>O<sub>3</sub>) formation during the anodizing process. The fourth column of Figures 5–7 corresponds to mapping the copper element present in the Al–Cu alloys of the anodized samples. This fourth column shows the copper content of the intermetallic phases, which can be the  $\delta$  (Al<sub>2</sub>CuMg) and  $\theta$  (Al<sub>2</sub>CuMg) phases.



**Figure 5.** Cross-section by SEM of anodized samples of AA2024 at 0.03 A/cm<sup>2</sup>: (a) 1MC, (e) 1MS, (i) 1MC 5S and (m) 1MC 10S. Mapping of element content; Aluminum (b,f,j,n), oxygen (c,g,k), and (o), Copper (d,h,l,p).

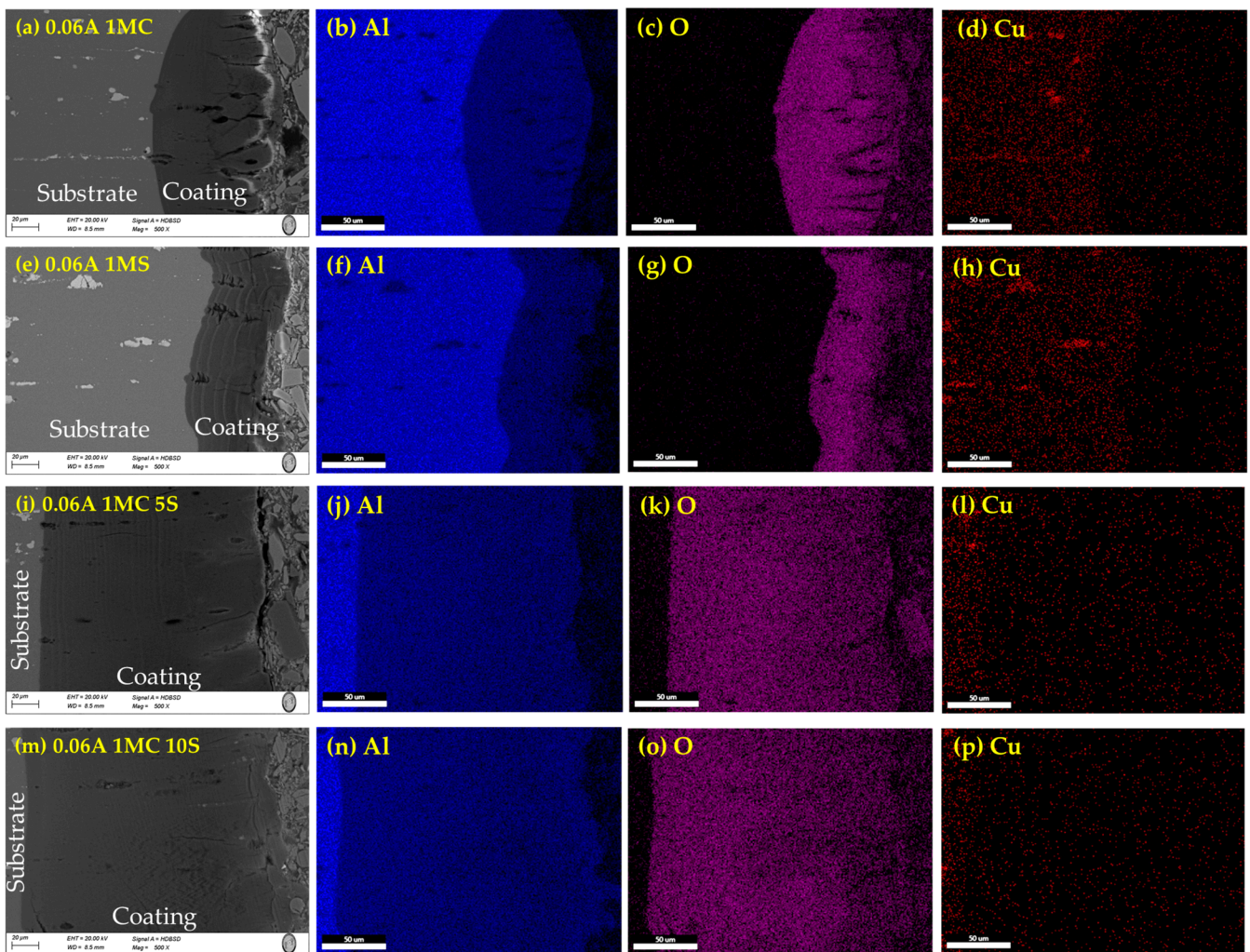




**Figure 6.** Cross-section by SEM of anodized samples of AA2024 at  $0.045 \text{ A/cm}^2$ : (a) 1MC, (e) 1MS, (i) 1MC 5S and (m) 1MC 10S. Mapping of element content; Aluminum (b,f,j,n), oxygen (c,g,k,o), Copper (d,h,l,p).

On the surface of anodized specimens 0.045A 1MC 5S, 0.045A 1MC 10S, 0.06A 1MC 5S, and 0.06A 1MC 10S, no porosity or cracking was observed (Figures 6i,m and 7i,m). These same figures show that these coatings are more homogeneous compared to the other samples and show less cracking. Anodized samples with a current density of  $0.03 \text{ A/cm}^2$  presented higher cracking in all anodizing solutions. Porosity and cracking were noted in samples 0.03A 1MS, 0.03A 1MC 5S, 0.045A 1MC, 0.045 1MS, 0.06A 1MC, and 0.06A 1MS (Figures 5e,i, 6a,e and 7a,e). In certain instances, these defects can penetrate the substrate from one side.

Microcracks typical of hard-anodized surfaces are discovered in different solutions, and current densities of the hard anodic coatings are generated [62]. Because the anodic coating and the metallic substrate have differing coefficients of thermal expansion, the sealing process creates thermal stresses that may result in pores and cracks on the materials' surface. Cracks and holes can also result from mechanical forces created during cross-sectional metallography preparation [63]. The samples that were anodized using solutions of sulfuric and citric acids showed no signs of porosity or cracks.



**Figure 7.** Cross-section by SEM of anodized samples of AA2024 at  $0.06 \text{ A/cm}^2$ : (a) 1MC, (e) 1MS, (i) 1MC 5S and (m) 1MC 10S. Mapping of element content; Aluminum (b,f,j,n), oxygen (c,g,k,o), Copper (d,h,l,p).

The lower thickness obtained in the 0.045A 1MC 5S and 0.045A 1MC 5S samples (Figure 6i,m) may be due to two reasons. The first is a dissolution of the aluminum oxide layer due to the low concentration of sulfuric acid in the anodizing solution, which has been reported by other researchers [39,64]. The second is a temperature increase in the anodizing process caused by the current supplied and the operating conditions of the process [65]. Additionally, cracking and detachment of the oxide layer could be caused by the metallographic preparation, which involves a heating process and increased pressure for the curing of the polymer resin (bakelite).

Al–Cu alloys contain the  $\theta$  phase ( $\text{Al}_2\text{Cu}$ ), and the behavior of the different second phases and the effect of the anodizing parameters on the properties of the anodic coatings are critical to realize an effective anodizing process [66]. Intermetallic precipitates strongly influence the morphology of anodic coatings and oxide growth. According to their composition, the copper-rich phases of the AA2024 Al alloy act as anodic zones for the case of the S-phase ( $\text{Al}_2\text{CuMg}$ ), while the  $\theta$ -phases ( $\text{Al}_2\text{Cu}$ ) act as cathodic zones, causing pitting corrosion in the material. The anodic oxides formed in aluminum alloys are not entirely composed of alumina due to the incorporation of alloying elements present in the substrate composition in the anodic layer and the incorporation of anions from the electrolyte. The effect of alloying elements on the anodized material's behavior and morphology depends on their nature. On this basis, alloying elements can be classified into three categories. The



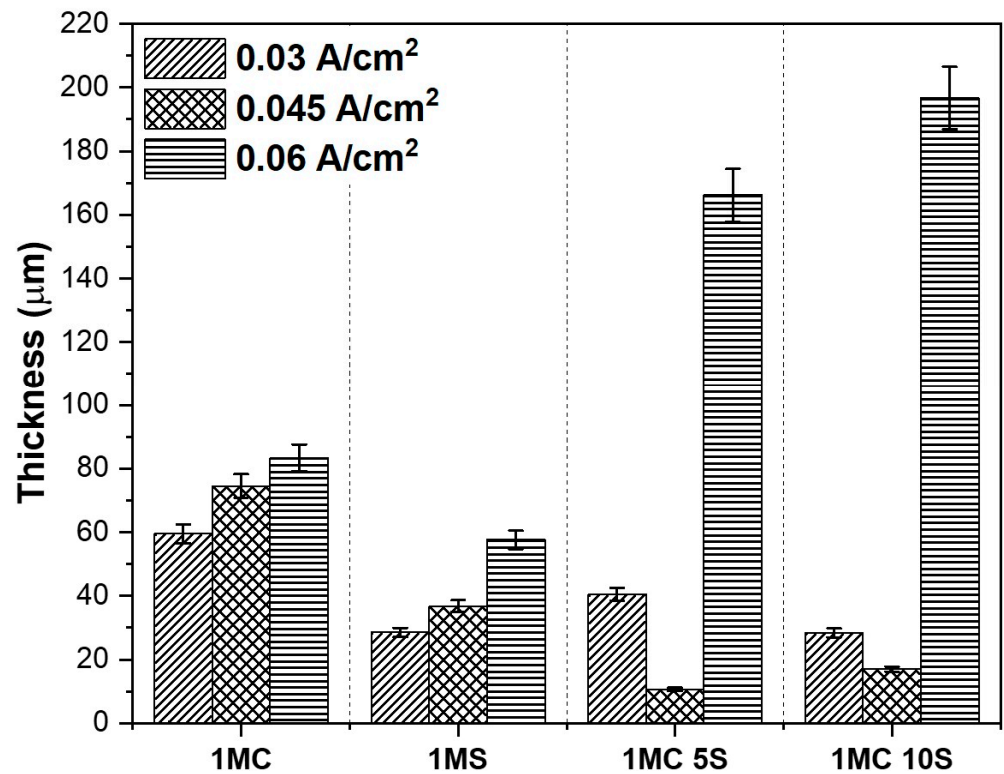
first category is alloying elements with a lower Gibbs free energy of oxide formation than aluminum oxide (e.g., Mg, Li). The second group consists of alloying elements slightly more noble than aluminum and that oxidize during the anodizing process (e.g., Zn, Cu). Finally, the third group consists of more noble elements than aluminum that do not undergo an oxidation process (e.g., Ag and Au) [67,68]. Since the alloys most used in the aerospace industry contain Mg, Cu, and Zn, attention should be paid to the effect of these elements on the oxide layer formed during anodizing.

Mg, being less noble than aluminum, oxidizes rapidly during the anodizing process, preferentially forming MgO since the volume occupied by MgO is smaller than the original volume occupied by elemental magnesium; the resulting oxide layer is not continuous and tends to detach [69,70]. When intermetallic Cu and CuO are present on the aluminum substrate, copper species are incorporated into the barrier-type anodic film as CuO units. In the first step, aluminum is preferentially oxidized at the oxide/alloy interface. The copper in solid solution and intermetallic phases such as the S-phase ( $\text{Al}_2\text{CuMg}$ ) and the  $\theta$ -phase ( $\text{Al}_2\text{Cu}$ ) is not oxidized. It accumulates under the anodic coating, giving rise to a copper-enriched zone. Copper particles are enriched below the anodic film and then incorporated into the anodic film because of the dealloying of the copper intermetallic phases during the anodizing process. When a certain threshold of copper content is reached, copper is oxidized, and  $\text{Al}_2\text{O}_3$ , MgO, and CuO are formed simultaneously.

On the other hand, aluminum oxide occupies a larger volume than elemental aluminum. It can fill the voids in the magnesium oxide, creating a continuous and well-bonded oxide film [71].  $\text{Al}_2\text{CuMg}$ ,  $\text{Al}_2\text{Cu}$ , and  $\text{Al}_7\text{Cu}_2\text{Fe}$  are copper intermetallic phases that show high activity with respect to the matrix and start oxidation at low potentials of 0, 1.8, and 2V vs. SCE [72]. Al–Cu alloys lose their anodizing effectiveness, and the oxygen produced destroys the layer when copper is incorporated into the film [73,74]. Cu, Mg, and Fe-rich intermetallic compounds and Si particles are the main factors impeding the anodic layer formation in Al alloys. These elements cause the anodized surface to show visually pleasing flaws in addition to reducing the oxide layers' surface mechanical qualities [75].  $\text{Mg}_2\text{Si}$ ,  $\beta\text{-Al}_5\text{FeSi}$ ,  $\alpha\text{-Al}(\text{Fe, Mn, Cr})\text{Si}$ , and  $\text{Al}_2\text{Cu}$  phases are examples of intermetallic complexes that are harmful to the anodization process [76,77]. The thickness of the oxide layer is influenced by these secondary phases, which also result in localized changes in the shape and composition of the interface between the bulk material and the oxide [70]. Furthermore, some phases may cause the anodic film porosity to increase while its hardness and thickness decrease [78].

### 3.2. Thickness of Anodized Materials

The cross-sectional thickness determined by SEM of the anodized samples of AA2024 at  $i = 0.03, 0.045, \text{ and } 0.06 \text{ A/cm}^2$  in various solutions of sulfuric and citric acid baths is shown in Figure 8. For the 1MC and 1MS solutions, it can be observed that the coating thickness increases as the anodizing current density increases. This behavior has been reported by some other authors, such as Benea et al. and Stepniowski et al., who obtained higher thicknesses of the oxide layer as the current density of the process increased [79,80]. The anodized samples 0.045A 1MC 5S and 0.045A 1MC 10S showed lower coating thicknesses, with 10.63 and 16.95  $\mu\text{m}$  values, respectively. The thicknesses of the other coatings were above 20  $\mu\text{m}$ . Samples 0.06A C1M 5S and 0.06A C1M 10S presented the highest thicknesses with 166.16 and 196.68  $\mu\text{m}$ , respectively. The coating is formed on the metal surface during the anodizing process, and depending on the coating thickness, current flows through the increasing layer to reach the clean metal surface. The oxidation film growth rate is directly impacted by the applied current density, which causes thickness variation. If the ideal value is surpassed, the film thickness may be decreased. An overly high current density will hasten the oxidation film's disintegration and increase the porosity heat effect [81–84].

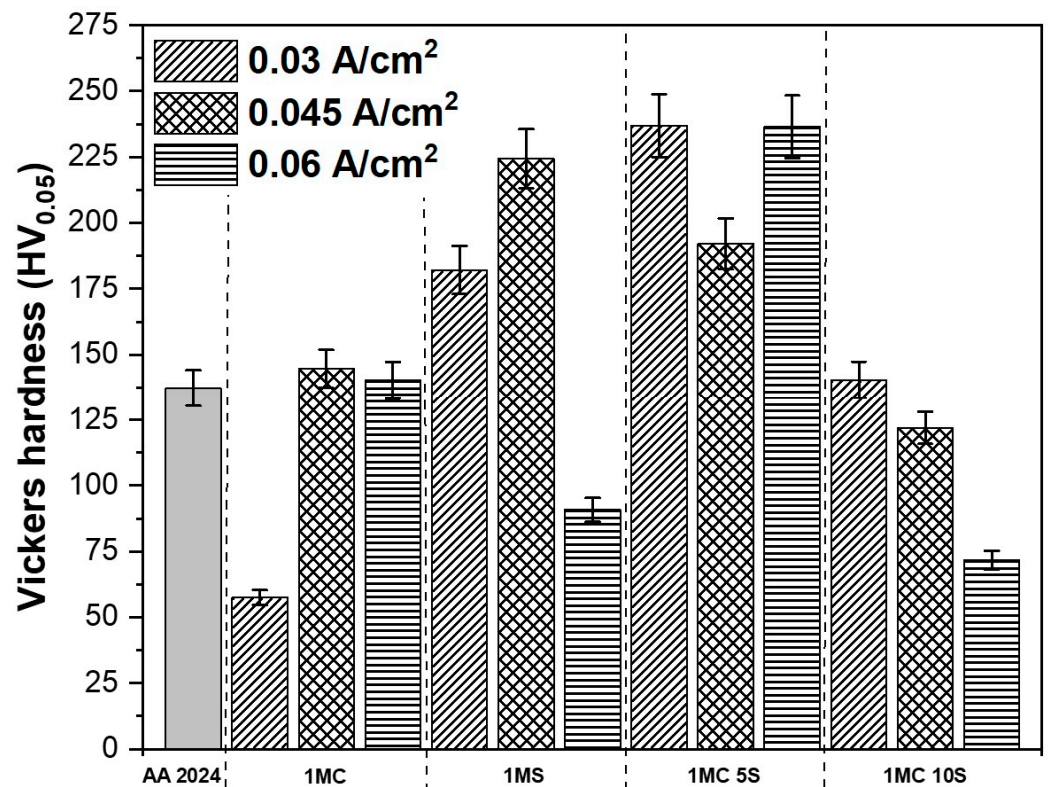


**Figure 8.** Coating thicknesses obtained vs. anodized AA2024 samples at 0.03, 0.045, and 0.06 A/cm<sup>2</sup>.

It has been observed that a noticeable breakdown of the anodic layer is generated when using sulfuric acid anodizing solution at low concentrations [85]. Electrolyte selection is given to perform an anodizing procedure that significantly impacts the produced anodic alumina film. Film characteristics will depend on the electrolyte's type, concentration, and temperature [86–88]. Military standards (Mil-A-8625) for hard anodizing specified a minimum thickness of 12.7 μm [89]. The thickness obtained in the different anodizing processes permitted greater thicknesses, but only samples 0.045 1MC 5S and 0.045 1MC 10S did not reach this thickness value.

### 3.3. Vickers Hardness

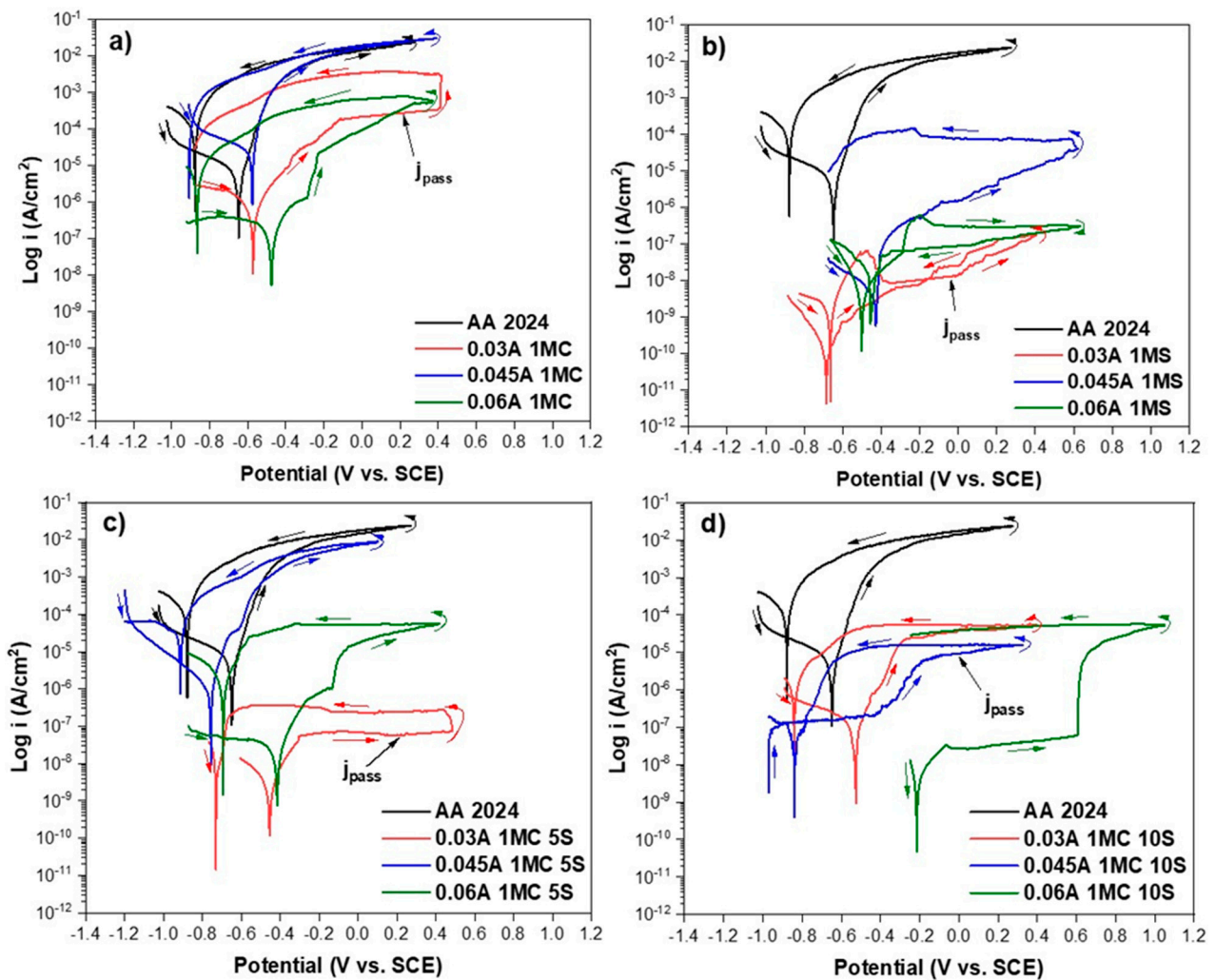
Figure 9 shows the results obtained from Vickers microhardness measurements. Maximum levels of microhardness were found in the 1MC 5S solution anodized samples at the different current densities of 0.03, 0.045 and 0.06 A/cm<sup>2</sup>, with values of 236.95, 192.14, and 236.53 HV, respectively. Samples 0.03A 1MC 10S, 0.045A 1MC, and 0.06A 1MC presented hardnesses like those shown by the base material AA 2024, which presented a value of 137.06 HV. Samples with lower hardness were 0.03A 1MC, 0.06A 1MS, and 0.06A 1MC 10S, with values of 57.48, 90.82, and 71.62 HV, respectively. This study did not obtain Vickers microhardness values greater than 300 HV, typical values for hard anodizing [3]. Some factors are the high temperatures; generally, the electrolytes used as baths for hard anodizing are solutions with higher concentrations; and the prolonged process times since they facilitate the disintegration of the film in the electrolyte, producing weaker and softer films that are powdery or easily detached [90].



**Figure 9.** Vickers microhardness measurements of AA2024 and anodized AA2024 samples at 0.03, 0.045, and 0.06 A/cm<sup>2</sup>.

### 3.4. Cyclic Potentiodynamic Polarization Curves (CPPC)

The corrosion kinetics behaviors of the anodized AA2024 were obtained through the potentiodynamic polarization curves. The CPPC curves were used to study the corrosion process, which provides information on the cathodic, anodic, and hysteresis branches of the anodized samples about the corrosion phenomena in the samples exposed to the 3.5 wt. % NaCl solution. The corrosion behavior of AA 2024 samples, both anodized and unanodized, in various solutions and with current densities of  $i = 0.03, 0.045,$  and  $0.06 \text{ A/cm}^2$  immersed in 3.5 wt. % NaCl solution is shown in Figure 10. The lowest corrosion potential is exhibited by AA2024 without anodizing, as shown in Figure 10a,  $E_{\text{corr}} = -0.656 \text{ V vs. SCE}$ , and presented corrosion current density of  $3.43 \times 10^{-7} \text{ A/cm}^2$ , all the other samples anodized in the different solutions presented more electropositive  $E_{\text{corr}}$ , sample 0.03A 1MC 5S is the one that presents better properties because its corrosion current density was the lowest of all the samples ( $j_{\text{corr}}$  of  $5.34 \times 10^{-9} \text{ A/cm}^2$ ), the samples anodized with citric-sulfuric acid with 5 and 10 mL/Liter presented similar characteristics and have better corrosion resistance than samples AA2024 and all samples present positive hysteresis indicating pitting corrosion. In Figure 10b, sample 0.03A 1MS has better properties because its achieved  $j_{\text{corr}} = 4.63 \times 10^{-9} \text{ A/cm}^2$ ) is one of the lowest samples analyzed in this work. Sample 0.06A 1MS achieved an  $E_{\text{corr}} = -0.501 \text{ V vs. SCE}$ , the highest of the anodized samples with a corrosion current density of  $1.29 \times 10^{-8} \text{ A/cm}^2$ . Lower susceptibility to corrosion is shown by the anodized samples' nobler values of  $E_{\text{corr}}$  [91,92].



**Figure 10.** CPPC of anodized AA2024 samples immersed in 3.5 wt. % NaCl solution using the same solutions and different current densities: (a) 1MC; (b) 1MS; (c) 1MC 5S; and (d) 1MC 10S.

In Figure 10c, all samples anodized with 5ml/liter sulfuric acid presented lower  $j_{\text{corr}}$  than those without anodizing. Sample 0.03A 1MC 5S and 0.06A 1MC 5S have lower corrosion current densities of  $5.31 \times 10^{-9}$  and  $5.01 \times 10^{-8}$  A/cm<sup>2</sup>, sample 0.045 1MC 5S has the lowest  $E_{\text{corr}} = -0.756$  V vs. SCE, and higher corrosion current density  $2.51 \times 10^{-6}$  A/cm<sup>2</sup>, or even than the non-anodized sample (AA2024) which obtained a value of  $-0.656$  V vs. SCE, all samples presented positive hysteresis loop. Finally, in Figure 10d again, all samples have lower  $j_{\text{corr}}$  than the unanodized sample AA2024, the lowest corrosion current density and the noblest  $E_{\text{corr}}$  was obtained in sample 0.06A 1MC 10S since  $j_{\text{corr}} = 5.76 \times 10^{-9}$  A/cm<sup>2</sup> and  $E_{\text{corr}} = -0.214$  V vs. SCE, were obtained. On the other hand, the lowest  $E_{\text{corr}}$  was of sample 0.045 1MC 10S with a value of  $-0.839$  V vs. SCE. The pitting potential ( $E_{\text{pit}}$ ) occurs at the vertex of the cyclic potentiodynamic polarization curve, this may be because the oxide surface is not homogeneous, as there are defects in the coatings (see Figures 2–4). At a potential lower than the oxygen evolution potential, the surface defects will be activated and start to propagate, which can increase the current density. Another reason is the presence of aggressive ions that increase the current density below the oxygen evolution, causing the anodic layer formed during the hard anodizing process to break down [93]. The samples that presented the anodic-cathodic potential ( $E_{\text{A-C}}$ ) as more negative than the corrosion potential ( $E_{\text{corr}}$ ), represent that its passive layer is not stable and can cause crevice corrosion [94]. This was present in all the samples with  $E_{\text{A-C}}$ . The corrosion parameters obtained from the CPPC shown in Table 3 are  $E_{\text{A-C}}$ ,  $E_{\text{corr}}$ , passivation current density ( $j_{\text{pass}}$ ),



pitting corrosion potential ( $E_{\text{pit}}$ ), corrosion current density ( $j_{\text{corr}}$ ), and hysteresis. Hard anodizing offers superior corrosion protection according to the values found for  $j_{\text{pass}}$  in the samples. This phenomenon is caused by the protective layer that forms in the anodizing and has a barrier effect; it has also been seen in AA7075 alloys anodized with different baths [95]. The corrosion resistance of various materials is directly correlated with  $j_{\text{corr}}$ . In this study, the lowest  $j_{\text{corr}}$  was obtained in samples 0.03A 1MC 5S, 0.045A 1MC 10S, 0.06A 1MC 5S, and 0.06A 1MC 10S, which were anodized in citric acid with sulfuric acid additions showing that hard anodizing can be fabricated with these types of baths. Samples anodized in sulfuric acid also exhibited low corrosion current densities, however, these samples are anodized in conventional sulfuric acid solutions. The highest  $j_{\text{corr}}$  were presented in samples 0.03A 1MC, 0.045A 1MC, and 0.06A 1MC, where the anodizing solution consisted completely of  $\text{C}_6\text{H}_8\text{O}_7$  (192 g in 1L of  $\text{H}_2\text{O}$ ). This behavior may be because as mentioned above the oxide layer in these samples was not homogeneous and galvanic couples may occur between the non-anodized (anodic sites) and anodized (cathodic sites) sections. The anodizing current density that presented the lowest  $j_{\text{corr}}$  regardless of the anodizing solution was 0.06 A/cm<sup>2</sup>, followed by 0.03 A/cm<sup>2</sup>. In the case of the anodizing current density of 0.06 A/cm<sup>2</sup> this behavior may be because the oxide layers obtained were among the thickest obtained, in the case of the anodizing current density of 0.03 A/cm<sup>2</sup> it may be attributed to the fact that these layers are more compact and with less cracking [96,97].

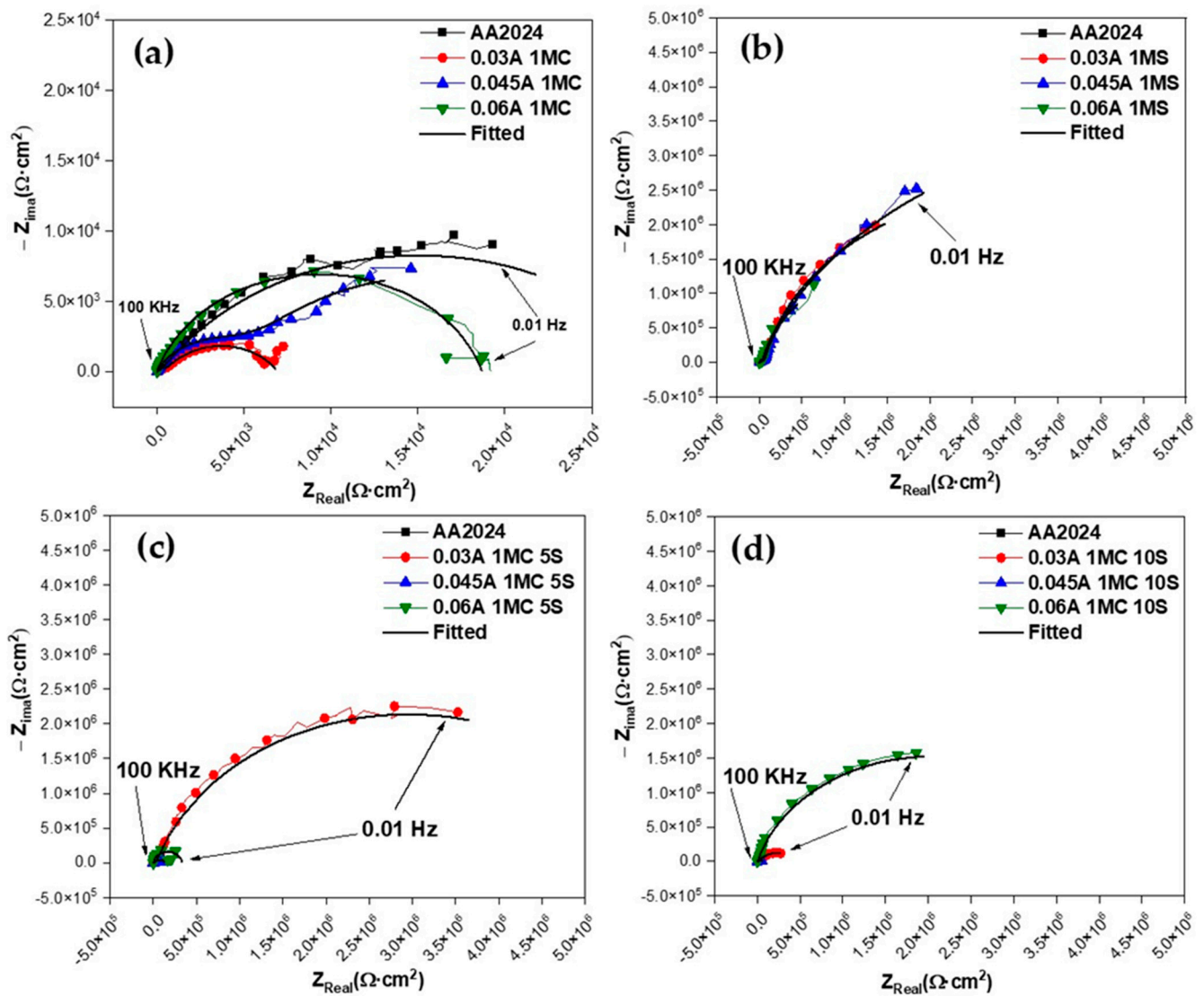
**Table 3.** Electrochemical parameters obtained from CPPC of AA 2024 and different samples anodized and immersed in 3.5 wt. % NaCl solution.

Samples	$E_{\text{corr}}$ (V vs. SCE)	$E_{\text{A-C}}$ (V vs. SCE)	$E_{\text{pit}}$ (V vs. SCE)	$j_{\text{pass}}$ (A/cm <sup>2</sup> )	$j_{\text{corr}}$ (A/cm <sup>2</sup> )	Hysteresis
AA2024	−0.656	−0.895	0.256	$3.35 \times 10^{-6} \pm 1.67 \times 10^{-7}$	$3.43 \times 10^{-7} \pm 1.71 \times 10^{-8}$	Positive
0.03A 1MC	−0.571	*	−0.411	$1.37 \times 10^{-8} \pm 6.85 \times 10^{-10}$	$1.50 \times 10^{-6} \pm 7.50 \times 10^{-8}$	Positive
0.03A 1MS	−0.664	−0.685	0.404	$5.34 \times 10^{-8} \pm 2.67 \times 10^{-9}$	$4.63 \times 10^{-9} \pm 2.31 \times 10^{-10}$	Positive
0.03A 1MC 5S	−0.453	−0.730	0.511	$3.97 \times 10^{-5} \pm 1.98 \times 10^{-6}$	$5.31 \times 10^{-9} \pm 2.65 \times 10^{-10}$	Positive
0.03A 1MC 10S	−0.526	−0.840	0.407	*	$1.04 \times 10^{-7} \pm 5.20 \times 10^{-9}$	Positive
0.045A 1MC	−0.577	−0.907	0.378	*	$4.83 \times 10^{-5} \pm 2.41 \times 10^{-6}$	Positive
0.045A 1MS	−0.431	*	0.611	*	$1.67 \times 10^{-8} \pm 8.35 \times 10^{-10}$	Positive
0.045A 1MC 5S	−0.756	−0.911	0.093	$1.28 \times 10^{-7} \pm 6.40 \times 10^{-9}$	$2.51 \times 10^{-6} \pm 1.25 \times 10^{-7}$	Positive
0.045A 1MC 10S	−0.839	−0.804	−0.411	*	$2.97 \times 10^{-7} \pm 1.48 \times 10^{-8}$	Positive
0.06A 1MC	−0.475	−0.865	0.368	$2.85 \times 10^{-7} \pm 1.42 \times 10^{-8}$	$2.58 \times 10^{-7} \pm 1.29 \times 10^{-8}$	Positive
0.06A 1MS	−0.501	−0.455	0.623	*	$1.29 \times 10^{-8} \pm 6.45 \times 10^{-10}$	Negative
0.06A 1MC 5S	−0.414	−0.692	0.421	$3.90 \times 10^{-8} \pm 1.95 \times 10^{-9}$	$5.01 \times 10^{-8} \pm 2.50 \times 10^{-9}$	Positive
0.06A 1MC 10S	−0.214	0.606	0.604	$3.35 \times 10^{-6} \pm 1.67 \times 10^{-7}$	$5.76 \times 10^{-9} \pm 2.88 \times 10^{-10}$	Positive

\* This value was not present in the corresponding curve.

### 3.5. Electrochemical Impedance Spectroscopy (EIS)

Figure 11 displays the features of the EIS spectra of the materials examined in this investigation. In addition to cyclic potentiodynamic polarization curves, EIS analysis was performed to provide a more thorough study of the corrosion susceptibility and protective properties of anodized materials. Figure 11a depicts the typical behavior of an oxide layer that naturally forms on the surface of aluminum alloys, such as AA2024, the sample that does not have an anodizing treatment [98,99]. There is a high-frequency semicircle and a capacitive behavior at lower frequencies for anodizing with the different citric-sulfuric acid mixtures and anodized current densities of 0.03 to 0.06 A/cm<sup>2</sup> (Figure 11a–d). These behaviors correspond to the properties of the barrier layer and the porous layer, respectively. Because of their depressed semicircles at high frequency ( $1 \times 10^2$ – $1 \times 10^4$  Hz), the anodized samples in citric acid solutions exhibit a reduced corrosion rate than the non-anodized AA2024 aluminum alloy, according to the Nyquist plot (Figure 11a).

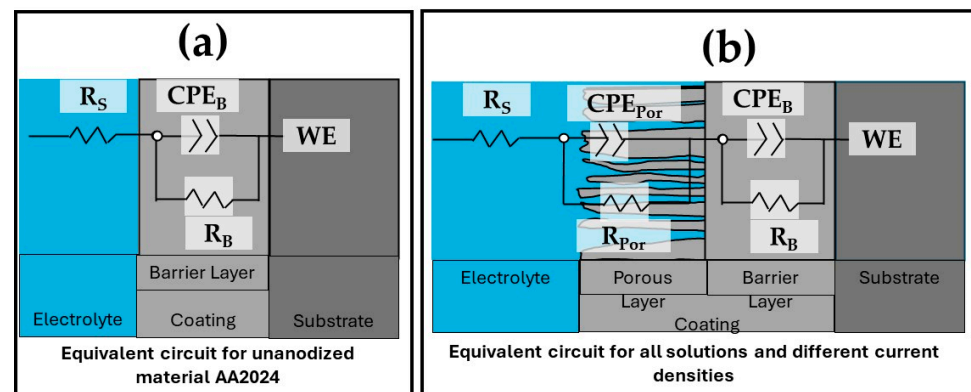


**Figure 11.** Nyquist plot for anodized AA2024 samples immersed in 3.5 wt. % NaCl solution using the same solutions and different current densities: (a) 1MC; (b) 1MS; (c) 1MC 5S; and (d) 1MC 10S.

The equivalent electrical circuits (EEC) proposed to model the combination of kinetic processes from the EIS tests are shown in Figure 12. In this EEC,  $R_s$  is the solution resistance,  $R_{Por}$  is the porous layer resistance, and  $R_B$  is the barrier layer resistance. Furthermore,  $CPE_{Por}$  is the constant phase element relative to the porous layer,  $CPE_B$  is the barrier layer constant phase element, and WE is the working electrode.  $n_{Por}$  and  $n_B$  are the impedance exponents to the porous and barrier layers, respectively. The roughness and variety of the porous and passive layers can be represented by the CPE. The parameter  $Z_{CPE}$  characterizes the impedance of a phase element, with  $Z_{CPE} = [C(i\omega)^n]^{-1}$ , where  $C$  is the capacitance;  $i$  is the current (imaginary number:  $-1^{0.5}$ );  $\omega$  is the angular frequency and  $-1 \leq n \leq 1$  [100,101]. A CPE with  $n = 1$  represents an ideal capacitor; and when  $0.5 < n < 1$ , a distribution of relaxation times in the frequency space is represented. It is also remarked that in order to compare simulated results with the experimented impedance data, CNLS (complex non-linear least squares) simulations were carried out. A ZView® (version 2.1b) software associated with two equivalent circuits is used to fit experimental data and chi-squared confirms its quality fitting [100,101]. The results of the simulations made with the corresponding equivalent electrical circuits in Figure 12 are shown in Table 4. Surface charge and the electrochemical double layer are related to coating morphology, which is what causes the variance in  $R_{Sol}$  [102]. Figure 11 shows the EEC model fit data,



which closely matches the experimental data. For this reason, most of the samples in Table 3 had error values in the range between 1.14 and 2.84, as indicated by the EEC simulations. Furthermore, the low values provided by  $\chi^2$  support the proposed EEC model's correctness. Considering the porous layer resistance ( $R_{Por}$ ) of all anodized samples with current densities of 0.03, 0.045, and 0.06 A/cm<sup>2</sup>. It can be established that such resistance ( $R_{Por}$ ) also contributes to the corrosion resistance of the anodized materials since the samples anodized in 1MS, 1MC 5S, and 1MC 10S solutions with the different anodizing current densities presented a higher  $R_{Por}$  than the barrier layer resistance ( $R_B$ ) presented by the non-anodized material. The anodized samples in 1MC solution did not show this behavior, however, the barrier layer resistance is higher for the 0.045A 1MC and 0.06A 1MC samples than the non-anodized material. The higher  $CPE_B$  values for the unanodized AA2024 and the samples anodized in 1MC solution are attributed to a thinner barrier layer. The results indicate that the thicknesses of these layers are more significant than the barrier layer formed naturally by the unanodized material, AA2024 (see Table 4). According to some authors, the capacitance of the formed layer decreases as the thickness of the formed layer increases [103–105]. This occurs for the samples anodized in 1MS, 1MC 5S, and 1MC 10S solutions with different anodizing current densities.



**Figure 12.** EEC from different samples=: (a) unanodized AA2024 and (b) all solutions and different current densities of anodizing.

In anodized materials, the corrosion resistance is inversely proportional to the charge transfer resistance ( $R_{ct}$ ), which relates to  $R_B$ . Analyzing the values of  $R_B$  of the samples un-anodizing AA2024, and anodized in 1MC solution with different current densities de 0.03, 0.045 y 0.06 A/cm<sup>2</sup> presented the lowest corrosion resistance in the evaluation medium with values that oscillate  $6.38 \times 10^3$  a  $19.47 \times 10^3 \Omega \cdot \text{cm}^2$ . In the anodized samples in solutions 1MS, 1MC 5S, and 1MC 10S,  $R_B$  values were increased, presenting values between  $140 \times 10^3$  and  $10,200 \times 10^3 \Omega \cdot \text{cm}^2$ , with different densities of anodizing current. The results of EIS indicate that the anodized citric–sulfuric acid mixtures have better corrosion resistance in the 3.5 wt. % NaCl solution than the material without anodized AA2024. The samples that presented higher  $R_B$  values were 0.045A 1MS, 0.06A 1MC 10S and 0.06A 1MC 5S, presenting values of  $10200 \times 10^3$ ,  $9680 \times 10^3$  and  $6260 \times 10^3 \Omega \cdot \text{cm}^2$ , respectively, providing excellent corrosion protection. These findings suggest that citric acid-based solutions can be used for the hard anodizing of aluminum alloys AA2024, reaching strength values equal to or higher than those documented in the literature for 6061 and 7075 aluminum alloys [106,107], and higher for those reported by Torato and Krusid, who reported strength values in anodized 2024 aluminum alloy in citric acid-sulfuric acid combinations between  $1380 \times 10^3 \Omega \cdot \text{cm}^2$  and  $2440 \times 10^3 \Omega \cdot \text{cm}^2$  [108]. Aluminum alloys are more resistant to corrosion when their metallic substrate has less porous and uniform surfaces, as this reduces the entry of chlorides towards the substrate [109,110]. The anodizing solutions utilized in this work, which consist of citric acid and modest amounts of sulfuric acid, efficiently shield aluminum alloys from corrosion and  $\text{Cl}^-$  ion attack.

**Table 4.** Electrochemical parameters obtained from Nyquist plot of AA 2024 and different samples anodized and immersed in 3.5 wt. % NaCl solution.

Samples	$R_S$ ( $\Omega \cdot \text{cm}$ )	$CPE_{Por}$ ( $F/\text{cm}^2$ )	$n_{Por}$	$R_{Por}$ ( $\Omega \cdot \text{cm}^2$ )	$CPE_B$ ( $F/\text{cm}^2$ )	$n_B$	$R_B$ ( $\Omega \cdot \text{cm}^2$ )	Error	$\chi^2$
AA2024	$28.5 \pm 1.42$	*	*	*	$127.00 \times 10^{-6} \pm 6.35 \times 10^{-6}$	0.80	$13.92 \times 10^3 \pm 0.69 \times 10^3$	<1.42	$1 \times 10^{-2}$
0.03A 1MC	$22.77 \pm 1.13$	$1.41 \times 10^{-6} \pm 7.05 \times 10^{-8}$	0.81	$0.56 \times 10^3 \pm 0.028 \times 10^3$	$40.20 \times 10^{-6} \pm 2.01 \times 10^{-6}$	0.64	$6.38 \times 10^3 \pm 0.31 \times 10^3$	<1.95	$3 \times 10^{-3}$
0.03A 1MS	$24.40 \pm 1.22$	$0.66 \times 10^{-6} \pm 3.34 \times 10^{-8}$	0.77	$152.00 \times 10^3 \pm 7.60 \times 10^3$	$0.84 \times 10^{-6} \pm 4.20 \times 10^{-8}$	0.94	$6200 \times 10^3 \pm 310 \times 10^3$	<1.79	$1 \times 10^{-2}$
0.03A 1MC 5S	$28.78 \pm 1.43$	$0.22 \times 10^{-6} \pm 1.14 \times 10^{-8}$	0.78	$46.00 \times 10^3 \pm 2.30 \times 10^3$	$0.93 \times 10^{-6} \pm 4.65 \times 10^{-8}$	0.81	$5810 \times 10^3 \pm 290 \times 10^3$	<1.96	$1 \times 10^{-2}$
0.03A 1MC 10S	$14.26 \pm 0.71$	$0.88 \times 10^{-6} \pm 4.40 \times 10^{-8}$	0.74	$47.00 \times 10^3 \pm 2.35 \times 10^3$	$3.12 \times 10^{-6} \pm 1.56 \times 10^{-7}$	0.69	$360 \times 10^3 \pm 18 \times 10^3$	<1.14	$1 \times 10^{-2}$
0.045A 1MC	$25.58 \pm 1.27$	$54.30 \times 10^{-6} \pm 2.71 \times 10^{-6}$	0.74	$6.55 \times 10^3 \pm 0.32 \times 10^3$	$481 \times 10^{-6} \pm 2.40 \times 10^{-5}$	0.71	$19.47 \times 10^3 \pm 0.97 \times 10^3$	<2.25	$1 \times 10^{-3}$
0.045A 1MS	$25.35 \pm 1.26$	$0.66 \times 10^{-6} \pm 3.32 \times 10^{-8}$	0.61	$89.00 \times 10^3 \pm 4.45 \times 10^3$	$1.26 \times 10^{-6} \pm 6.30 \times 10^{-8}$	0.91	$10200 \times 10^3 \pm 510 \times 10^3$	<2.17	$7 \times 10^{-3}$
0.045A 1MC 5S	$63.58 \pm 3.17$	$0.11 \times 10^{-6} \pm 5.65 \times 10^{-9}$	0.85	$2.00 \times 10^3 \pm 0.10 \times 10^3$	$6.11 \times 10^{-6} \pm 3.05 \times 10^{-7}$	0.54	$140 \times 10^3 \pm 7 \times 10^3$	<2.84	$1 \times 10^{-2}$
0.045A 1MC 10S	$16.88 \pm 0.84$	$2.27 \times 10^{-6} \pm 1.13 \times 10^{-7}$	0.75	$15.00 \times 10^3 \pm 0.75 \times 10^3$	$1.26 \times 10^{-6} \pm 6.30 \times 10^{-8}$	0.90	$4110 \times 10^3 \pm 205 \times 10^3$	<2.04	$3 \times 10^{-2}$
0.06A 1MC	$20.48 \pm 1.02$	$2.19 \times 10^{-6} \pm 1.09 \times 10^{-7}$	0.82	$7.70 \times 10^3 \pm 0.38 \times 10^3$	$2.36 \times 10^{-6} \pm 1.18 \times 10^{-7}$	0.89	$18.31 \times 10^3 \pm 0.91 \times 10^3$	<1.48	$1 \times 10^{-3}$
0.06A 1MS	$76.47 \pm 3.82$	$0.34 \times 10^{-6} \pm 1.74 \times 10^{-8}$	0.69	$34.00 \times 10^3 \pm 1.70 \times 10^3$	$1.73 \times 10^{-6} \pm 8.65 \times 10^{-8}$	0.88	$3470 \times 10^3 \pm 173 \times 10^3$	<1.31	$3 \times 10^{-3}$
0.06A 1MC 5S	$10.61 \pm 0.53$	$8.39 \times 10^{-6} \pm 4.19 \times 10^{-7}$	0.61	$52.00 \times 10^3 \pm 2.60 \times 10^3$	$3.48 \times 10^{-6} \pm 1.74 \times 10^{-7}$	0.70	$6250 \times 10^3 \pm 312 \times 10^3$	<1.25	$2 \times 10^{-2}$
0.06A 1MC 10S	$87.69 \pm 4.38$	$0.35 \times 10^{-6} \pm 1.78 \times 10^{-8}$	0.69	$40.00 \times 10^3 \pm 2.00 \times 10^3$	$1.43 \times 10^{-6} \pm 7.15 \times 10^{-8}$	0.87	$9680 \times 10^3 \pm 484 \times 10^3$	<2.21	$2 \times 10^{-3}$

\* This value was not present in the corresponding sample.

#### 4. Conclusions

- The results indicate that anodic alumina films exhibiting good mechanical qualities and corrosion resistance, like traditional anodizing in H<sub>2</sub>SO<sub>4</sub>, were effectively generated under hard anodizing conditions in AA 2024 aluminum–copper alloy utilizing citric-sulfuric acid solutions.
- Most anodized samples showed cracking and surface porosity regardless of the anodizing solution and current density used, this behavior may be due to the different temperatures used between anodizing (0 °C) and sealing (95 °C). However, samples 0.06 A/cm<sup>2</sup> 1MC 5S and 0.06 A/cm<sup>2</sup> 1MC 10S present their defects with a different nature than the other anodized samples.
- The SEM results indicated that in the cross-section of the coatings, there was cracking and porosity related to the sealing process due to differences in the coefficient of thermal expansion of the substrate/coating.
- The anodizing carried out in mixtures composed of citric-sulfuric acid and current densities of 0.03 and 0.06 A/cm<sup>2</sup> can be achieved with thicknesses from 25 to 196 μm.
- Most of the anodized AA2024 aluminum–copper samples with a current density of 0.045 A/cm<sup>2</sup> obtained a Vickers microhardness above 137 HV, higher than that of the non-anodized AA2024 sample.
- Cyclic potentiodynamic polarization curves indicated that samples anodized in citric-sulfuric acid produced values comparable to conventional sulfuric acid anodizing in terms of lowest corrosion current densities ( $j_{\text{corr}}$ ).
- EIS results showed that hard anodized coatings made with citric-sulfuric acid mixtures showed greater corrosion resistance when exposed to a corrosive of 3.5 wt. %NaCl solution, with resistance values of  $5810 \times 10^3 \pm 290 \times 10^3$  and  $9680 \times 10^3 \pm 484 \times 10^3 \Omega \cdot \text{cm}^2$  for samples 0.03A 1MC 5S and 0.06A 1MC 10S, respectively.
- With anodizing in citric-sulfuric acid solutions, savings of 190 mL of H<sub>2</sub>SO<sub>4</sub> can be obtained by substituting it for citric acid and achieving similar anodizing properties.
- Samples anodized at current densities of 0.03 and 0.06 A/cm<sup>2</sup> presented the lowest corrosion current densities due to the characteristics presented by the coatings.
- In the anodized process, the current density used has an important effect on the morphology, thickness, and structure of the anodized layer. Although, it is also important to consider the time spent in the anodizing bath, the temperature, and the stirring system, which can be variables that influence the defects of the anodized layer.

**Author Contributions:** In this work, Conceptualization, J.C.-M. and F.A.C. methodology, D.N.-M., F.E.-L., N.C.-M.; E.M.-B. and M.L.-B.; data curation, E.M.-B., J.O.-C., D.N.-M., J.C.-M., N.C.-M. and L.D.L.-L.; formal analysis, F.A.C., L.D.L.-L., M.L.-B. and C.G.T.; validation, J.C.-M. and F.A.C.; writing—original draft preparation, J.C.-M., C.G.T. and J.C.-M.; writing—review and editing, J.C.-M. and F.A.C. All authors have read and agreed to the published version of the manuscript.

**Funding:** This research was funded by the Universidad Autónoma de Nuevo León (UANL).

**Institutional Review Board Statement:** Not applicable.

**Informed Consent Statement:** Not applicable.

**Data Availability Statement:** Data are contained within the article.

**Acknowledgments:** The authors acknowledge The Academic Body UANL—CA-316 “Deterioration and integrity of composite materials” and Jesus Manuel Jaquez, for your English revision.

**Conflicts of Interest:** The authors declare no conflicts of interest.

#### References

1. Abdel-Salam, O.E.; Shoeib, M.A.; Elkilany, H.A. Characterization of the hard anodizing layers formed on 2014-T3 Al alloy, in sulphuric acid electrolyte containing sodium lignin sulphonate. *Egypt. J. Petrol.* **2017**, *27*, 497–504. [[CrossRef](#)]
2. Bethencourt, M.; Botana, F.J.; Cano, M.J.; Marcos, M.; Sánchez-Amaya, J.M.; González-Rovira, L. Behavior of the alloy AA2017 in aqueous solutions of NaCl. Part I: Corrosion mechanisms. *Corr. Sci.* **2023**, *51*, 518–524. [[CrossRef](#)]

3. Kwolek, P. Hard Anodic Coatings on Aluminum Alloys. *Adv. Manuf. Sci. Tech.* **2017**, *41*, 35–46.
4. Davis, J. *Aluminum and Aluminum Alloys, Prepared under the Direction of the ASM International Handbook Committee*; ASM International: Metals Park, OH, USA, 1994; pp. 231–267.
5. Mouritz, P.A. Aluminium Alloys for Aircraft Structures. In *Introduction to Aerospace Materials*, 1st ed.; Mouritz, P.A., Ed.; Woodhead Publishing: Boston, MA, USA, 2012; Volume 1, pp. 173–201.
6. Gloria, A.; Nontanari, R.; Richetta, M.; Varone, A. Alloys for Aeronautic Applications: State of the Art and Perspectives. *Metals* **2019**, *9*, 662. [CrossRef]
7. Applications of 2024 Aluminum Alloy. Available online: <https://www.howardprecision.com/applications-of-2024-aluminum-alloy/> (accessed on 11 July 2022).
8. Huda, Z.; Taib, N.I.; Zaharinie, T. Characterization of 2024-T3: An aerospace aluminum alloy. *Mater. Chem. Phys.* **2009**, *113*, 515–517. [CrossRef]
9. Lacroix, L.; Blanc, C.; Pébère, N.; Thompson, G.E.; Tribollet, B.; Vivier, V. Simulating the galvanic coupling between S-Al<sub>2</sub>CuMg phase particles and the matrix of 2024 aerospace aluminium alloy. *Corros. Sci.* **2012**, *64*, 213–221. [CrossRef]
10. Technical Report TR-17. In *Hard Anodizing of Aluminum Alloys and Its Effect on Bal Seal Performance*; Bal Seal Engineering, Inc.: Lake Forest, CA, USA, 2016. Available online: [https://www.balseal.com/wp-content/uploads/2019/06/Effects\\_Of\\_Hard\\_Anodizing\\_Aluminum\\_Alloys\\_On\\_Bal\\_SealTR\\_17.pdf](https://www.balseal.com/wp-content/uploads/2019/06/Effects_Of_Hard_Anodizing_Aluminum_Alloys_On_Bal_SealTR_17.pdf) (accessed on 11 July 2022).
11. Cotell, C.M. Surface Engineering of Aluminum and Aluminum Alloys. In *ASM Handbook*; ASM International: Metals Park, OH, USA, 1994; Volume 5, pp. 4–7.
12. Gabe, D.R. Hard anodizing—What do we mean by hard? *Met. Finish.* **2002**, *100*, 52–58. [CrossRef]
13. Roshani, M.; Rouhaghdam, A.S.; Aliofkhaezraei, M.; Astaraee, A.H. *Optimization of Mechanical Properties for Pulsed Anodizing of Aluminum*; Elsevier BV Department of Materials Engineering: Amsterdam, The Netherlands, 2016; pp. 14115–14143.
14. Sheasby, P.G.; Pinner, R. *The Surface Treatment and Finishing of Aluminium and Its Alloys*, 6th ed.; Finishing Publications Limited: Warrington, UK; ASM International: Almere, The Netherlands, 2001; Volume 1, pp. 427–535.
15. Chung, I.C.; Chung, C.K.; Su, Y.K. Effect of current density and concentration on microstructure and corrosion behavior of 6061 Al alloy in sulfuric acid. *Surf. Coat. Technol.* **2017**, *3133*, 299–306. [CrossRef]
16. Lu, J.; Wei, G.; Yu, Y.; Guo, C.; Jiang, L. Aluminum alloy AA2024 anodized from the mixed acid system with enhanced mechanical properties. *Surf. Interface* **2018**, *13*, 46–50. [CrossRef]
17. Mezlini, S.; Elleuch, K.; Kapsa, P. The effect of sulphuric anodization of aluminum alloys on contact problems. *Surf. Coat. Technol.* **2006**, *200*, 2852–2856. [CrossRef]
18. Martínez-Viademonte, M.; Abrahami, S.T.; Hack, T.; Burchardt, M.; Terryn, H. A Review on Anodizing of Aerospace Aluminum Alloys for Corrosion Protection. *Coatings* **2020**, *10*, 1106. [CrossRef]
19. Thompson, G. Porous anodic alumina: Fabrication, characterization and applications. *Thin Solid Film.* **1997**, *297*, 192–201. [CrossRef]
20. Memerifard, S.; Rahimpour, M.; Mobashrpour, I. Investigation of organic additives on voltage rate in aluminum hard-anodizing process. *Int. J. Bio-Inorg. Hybr. Nanomater.* **2017**, *6*, 59–63.
21. Brace, A.W. *The Technology of Anodizing Aluminum*; Interall, S.r.l.: Modena, Italy, 2000.
22. Renaud, A.; Paint, Y.; Lanzutti, A.; Bonnaud, L.; Fedrizzi, L.; Dubois, P.; Poorteman, M.; Oliver, M.G. Sealing porous anodic layers on AA2024-T3 with a low viscosity benzoxazine resin for corrosion protection in aeronautical applications. *RSC Adv.* **2019**, *9*, 16819–16830. [CrossRef] [PubMed]
23. Norek, M.; Wlodarski, M. Morphological and chemical characterization of highly ordered conical-pore anodic alumina prepared by multistep citric acid anodizing and chemical etching process. *J. Porous Mater.* **2018**, *25*, 45–53. [CrossRef]
24. Shoshan, T.A.; De Kok, J.M.M.; Terryn, H.; Mol, J.M.C. Towards Cr (VI)-free anodization of aluminum alloys for aerospace adhesive bonding applications: A review. *Front. Chem. Sci. Eng.* **2017**, *11*, 465–482.
25. Abd El-Hameed, A.M.; Abdel-Aziz, Y.A.; El-Tokhy, F.S. Anodic Coating Characteristics of Different Aluminum Alloys for Spacecraft Materials Applications. *Mat. Sci. Appl.* **2017**, *8*, 197–208. [CrossRef]
26. Nakajima, D.; Kikuchi, T.; Natsui, S.; Suzuki, R.O. Growth behavior of anodic oxide formed by aluminum anodizing in glutaric and its derivative acid electrolytes. *Appl. Surf. Sci.* **2014**, *321*, 364–370. [CrossRef]
27. Jalal, H.; Saoud, Y.; Karabet, F. Effect of organic additives on AA6066 anodization. *J. Chem. Technol. Metall.* **2019**, *54*, 447–453.
28. Cabral-Miramontes, J.; Almeraya-Calderón, F.; López, F.E.; Lara Banda, M.; Olguín-Coca, J.; López-León, L.D.; Castañeda-Robles, I.; Alcalá, M.Á.E.; Zambrano-Robledo, P.; Gaona-Tiburcio, C. Citric Acid as an Alternative to Sulfuric Acid for the Hard-Anodizing of AA6061. *Metals* **2021**, *11*, 1838. [CrossRef]
29. Solmaz, R.; Kardas, G.; Yazici, B.; Erbil, M. Citric acid as natural corrosion inhibitor for aluminum protection. *Corros. Eng. Sci. Technol.* **2008**, *43*, 186–191. [CrossRef]
30. Martell, A.E.; Smith, R.M. *Critical Stability Constants*; Plenum Press: New York, NY, USA, 1976; Volume 1–4.
31. Stepniowski, W.J.; Norek, M.; Michalska-Domańska, M.; Bombalska, A.; Nowak-Stepniowska, A.; Kwaśny, M.; Bojar, Z. Fabrication of anodic aluminum oxide with incorporated chromate ions. *Appl. Surf. Sci.* **2012**, *259*, 324–330. [CrossRef]
32. Stepniowski, W.J.; Michalska-Domańska, M.; Norek, M.; Czujko, T. Fast Fourier transform based arrangement analysis of poorly organized alumina nanopores formed via self-organized anodization in chromic acid. *Mater. Lett.* **2014**, *117*, 69–73. [CrossRef]

33. Le Coz, F.; Arurault, L.; Fontorbes, S.; Vilar, V.; Datas, L.; Winterton, P. Chemical composition and structural changes of porous templates obtained by anodising aluminium in phosphoric acid electrolyte. *Surf. Interface Anal.* **2010**, *42*, 227–233. [[CrossRef](#)]
34. Masuda, H.; Yada, K.; Osaka, A. Self-ordering of cell configuration of anodic porous alumina with large-size pores in phosphoric acid solution. *Jpn. J. Appl. Phys.* **1998**, *37*, L1340. [[CrossRef](#)]
35. Guthrie, P.J. Hydrolysis of esters of oxy acids: pKa values for strong acids; Brønsted relationship for attack of water at methyl; free energies of hydrolysis of esters of oxy acids; and a linear relationship between free energy of hydrolysis and pKa holding over a range of 20 pK units. *Can. J. Chem.* **2011**, *56*, 2342–2354. [[CrossRef](#)]
36. Poznyak, A.; Pligovka, A.; Laryn, T.; Salerno, M. Porous Alumina Films Fabricated by Reduced Temperature Sulfuric Acid Anodizing: Morphology, Composition and Volumetric Growth. *Materials* **2021**, *14*, 767. [[CrossRef](#)] [[PubMed](#)]
37. De Graeve, I.; Terryn, H.; Thompson, G.E. Influence of local heat development on film thickness for anodizing aluminum in sulfuric acid. *J. Electrochem. Soc.* **2003**, *150*, B158–B165. [[CrossRef](#)]
38. Cabral-Miramontes, J.; Gaona-Tiburcio, C.; Estupiñan-López, F.; Lara-Banda, M.; Zambrano-Robledo, P.; Nieves-Mendoza, D.; Bandala, E.M.; Nava, J.C.; Almeraya-Calderón, F. Corrosion Resistance of Hard Coat Anodized AA 6061 in Citric-Sulfuric Solutions. *Coatings* **2020**, *10*, 601. [[CrossRef](#)]
39. Poznyak, A.; Pligovka, A.; Turavets, U.; Norek, M. On-aluminum and barrier anodic oxide: Meeting the challenges of chemical dissolution rate in various acids and solutions. *Coatings* **2020**, *10*, 875. [[CrossRef](#)]
40. Cabral Miramontes, J.C.; Gaona Tiburcio, C.; García Mata, E.; Esneider Alcála, M.Á.; Maldonado-Bandala, E.; Lara-Banda, M.; Nieves-Mendoza, D.; Olguín-Coca, J.; Zambrano-Robledo, P.; López-León, L.D.; et al. Corrosion Resistance of Aluminum Alloy AA2024 with Hard Anodizing in Sulfuric Acid-Free Solution. *Materials* **2022**, *15*, 6401. [[CrossRef](#)]
41. Sulka, G.D.; Brzózka, A.; Zaraska, L.; Jaskuła, M. Through-hole membranes of nanoporous alumina formed by anodizing in oxalic acid and their applications in fabrication of nanowire arrays. *Electrochim. Acta* **2010**, *55*, 4368–4376. [[CrossRef](#)]
42. Stepniowski, W.J.; Nowak-Stepniowska, A.; Bojar, Z. Quantitative arrangement analysis of anodic alumina formed by short anodizations in oxalic acid. *Mater. Charact.* **2013**, *78*, 79–86. [[CrossRef](#)]
43. Ren, J.; Zuo, Y. The anodizing behavior of aluminum in malonic acid solution and morphology of the anodic films. *Appl. Surf. Sci.* **2012**, *261*, 193–200. [[CrossRef](#)]
44. Vrublevsky, I.; Jagminas, A.; Hemeltjen, S.; Goedel, W. Behavior of acid species during heat treatment and re-anodizing of porous alumina films formed in malonic acid. *J. Solid State Electrochem.* **2009**, *13*, 1873–1880. [[CrossRef](#)]
45. Chu, S.Z.; Wada, K.; Inoue, S.; Isogai, M.; Katsuta, Y.; Yasumori, A. Large-scale fabrication of ordered nanoporous alumina films with arbitrary pore intervals by critical-potential anodization. *J. Electrochem. Soc.* **2006**, *153*, B384–B391. [[CrossRef](#)]
46. Vrublevsky, I.A.; Chernyakova, K.V.; Ispas, A.; Bund, A.; Zavadski, S. Optical properties of thin anodic alumina membranes formed in a solution of tartaric acid. *Thin Solid Film.* **2014**, *556*, 230–235. [[CrossRef](#)]
47. ASTM G61-86; Standard Test Method for Conducting Cyclic Potentiodynamic Polarization Measurements for Localized Corrosion Susceptibility of Iron-, Nickel-, or Cobalt-Based Alloys. ASTM International: West Conshohocken, PA, USA, 2018.
48. ASTM G106-15; Standard Practice for Verification of Algorithm and Equipment for Electrochemical Impedance Measurements. ASTM International: West Conshohocken, PA, USA, 2015.
49. ASTM E3-95; Standard Practice for Preparation of Metallographic Specimens. ASTM International: West Conshohocken, PA, USA, 1995.
50. ASTM E407-07; Standard Practice for Microetching Metals and Alloys. ASTM International: West Conshohocken, PA, USA, 2011.
51. Martínez-Villafaña, A.; Almeraya-Calderón, M.F.; Gaona-Tiburcio, C.; Gonzalez-Rodriguez, J.G.; Porcayo-Calderón, J. High-Temperature Degradation and Protection of Ferritic and Austenitic Steels in Steam Generators. *J. Mater. Eng. Perform.* **1997**, *7*, 108–113. [[CrossRef](#)]
52. Zhou, M. Aluminum room temperature hard anodizing technology. Mechanism of organic additives and bath liquid maintenance. *Plat. Environ. Protect.* **2002**, *22*, 28–30.
53. Franco, M.; Krishna, T.H.; Pillai, A.M.; Rajendra, A.; Sharma, A.K. A comparative study on the corrosion behavior of hard anodic coatings on AA 6061 obtained using dc and pulsed dc power sources. *Acta Metall. Sin. Engl. Lett.* **2013**, *26*, 647–656. [[CrossRef](#)]
54. Gazapo, J.L.; Gea, J. *Anodizing of Aluminium*; European Aluminium Association: Alicante, Spain, 1994; pp. 1–27.
55. ASTM E92-17; Standard Test Method for Vickers Hardness of Metallic Materials. ASTM International: West Conshohocken, PA, USA, 2017.
56. Ma, Y.; Wen, Y.; Li, J.; Lu, J.; Li, Y.; Yang, Y.; Feng, C.; Hao, C.; Zhang, Z.; Hu, J.; et al. Pore nucleation mechanism of self-ordered alumina with large period in stable anodization in citric acid. *J. Electrochem. Soc.* **2018**, *165*, E311–E317. [[CrossRef](#)]
57. Tabesh, S.; Davar, F.; Loghman-Estarki, M.R. The effects of chelating agent type on the morphology and phase evolutions of alumina nanostructures. *Ceram. Int.* **2017**, *43*, 10247. [[CrossRef](#)]
58. Soffritti, C.; Fortini, A.; Nastruzzi, A.; Sola, R.; Merlin, M.; Garagnani, G.L. Dry Sliding Behavior of an Aluminum Alloy after Innovative Hard Anodizing Treatments. *Materials* **2021**, *14*, 3281. [[CrossRef](#)] [[PubMed](#)]
59. Guezmil, M.; Bensalah, W.; Khalladi, A.; Elleuch, K.; Depetris-Wery, M.; Ayedi, H.F. Friction coefficient and microhardness of anodized aluminum alloys under different elaboration conditions. *Trans. Non-Ferr. Met. Soc. China* **2015**, *25*, 1950–1960. [[CrossRef](#)]
60. López, V.; Otero, E.; Bautista, A.; González, J.A. Sealing of anodic films obtained in oxalic acid baths. *Surf. Coat. Technol.* **2000**, *124*, 76–84. [[CrossRef](#)]



61. Van Der Linden, B.; Terryn, H.; Vereecken, J. Investigation of anodic aluminium oxide layers by electrochemical impedance spectroscopy. *J. Appl. Electrochem.* **1990**, *20*, 798–803. [[CrossRef](#)]
62. Almeraya-Calderon, F.; Villegas-Tovar, M.; Maldonado-Bandala, E.; Lara-Banda, M.; Baltazar-Zamora, M.A.; Santiago-Hurtado, G.; Nieves-Mendoza, D.; Lopez-Leon, L.D.; Jaquez-Muñoz, J.M.; Estupiñán-López, F.; et al. Use of Electrochemical Noise for the Study of Corrosion by Passivated CUSTOM 450 and AM 350 Stainless Steels. *Metals* **2024**, *14*, 341. [[CrossRef](#)]
63. Moutarlier, V.; Gigandet, M.P.; Ricq, L.; Pagetti, J. Electrochemical characterization of anodic oxidation films formed in presence of corrosion inhibitors. *Appl. Surf. Sci.* **2001**, *183*, 1–9. [[CrossRef](#)]
64. Schneider, M.; Liebmann, T.; Langklotz, U.; Michaelis, A. Microelectrochemical investigation of anodic oxide formation on the aluminum alloy AA2024. *Electrochim. Acta* **2017**, *249*, 198–205. [[CrossRef](#)]
65. Peng, L.; Li, M. Improved technology for hard anodizing dissolution of aluminum alloy part. *Open Mat. Sci. J.* **2015**, *9*, 82–85. [[CrossRef](#)]
66. Vukmirovic, M.B.; Dimitrov, N.; Sieradzki, K. Dealloying and corrosion of Al alloy 2024 T3. *J. Electrochem. Soc.* **2002**, *149*, 428–439. [[CrossRef](#)]
67. Habazaki, H.; Shimizu, K.; Skeldon, P.; Thompson, G.E.; Wood, G.C. The composition of the alloy/film interface during anodic oxidation of Al-W alloys. *J. Electrochem. Soc.* **1996**, *143*, 2465–2470. [[CrossRef](#)]
68. Habazaki, H.; Shimizu, K.; Skeldon, P.; Thompson, G.E.; Wood, G.C.; Zhou, X. Effects of alloying elements in anodizing of aluminium. *Trans IMF.* **1997**, *75*, 18–23. [[CrossRef](#)]
69. Habazaki, H.; Zhou, X.; Shimizu, K.; Skeldon, P.; Thompson, G.E.; Wood, G.C. Mobility of copper ions in anodic alumina films. *Electrochim. Acta.* **1997**, *42*, 2627–2635. [[CrossRef](#)]
70. Torrescano-Alvarez, J.M.; Curioni, M.; Habazaki, H.; Hashimoto, T.; Skeldon, P.; Zhou, X. Incorporation of alloying elements into porous anodic films on aluminium alloys: The role of cell diameter. *Electrochim. Acta* **2019**, *296*, 783–789. [[CrossRef](#)]
71. Michalska-Domańska, M.; Norek, M.; Stepniowski, W.J.; Budner, B. Fabrication of high quality anodic aluminum oxide (AAO) on low purity aluminum-A comparative study with the AAO produced on high purity aluminum. *Electrochim. Acta* **2013**, *105*, 424–432. [[CrossRef](#)]
72. Saenz de Miera, M.; Curioni, M.; Skeldon, P.; Thompson, G.E. Modelling the anodizing behavior of aluminum alloys in sulfuric acid through alloy analogues. *Corros. Sci.* **2008**, *50*, 3410–3415. [[CrossRef](#)]
73. Iglesias-Rubianes LGarcia-Vergara, S.J.; Skeldon, P.; Thompson, G.E.; Ferguson, J.; Beneke, M. Cyclic oxidation processes during anodizing of Al–Cu alloys. *Electrochim. Acta* **2007**, *52*, 7148–7157. [[CrossRef](#)]
74. Arenas, M.A.; Skeldon, P.; Thompson, G.E.; Bailey, P.; Noakes, T.C.Q.; Habazaki, H.; Shimizu, K. Anodic behavior of a model second phase: Al–20 at.% Mg–20 at.% Cu. *Corros. Sci.* **2006**, *48*, 1225–1248.
75. Caliarì, D.; Timelli, G.; Salata, T.; Cavagnini, G.; Maestri, S. Surface defects of anodized HPDC Al alloy components. *Metall. Ital.* **2016**, *108*, 69–72.
76. Tsangaraki-Kaplanoglou, I.; Theohari, S.; Dimogerontakis, T.; Wang, Y.M.; Kuo, H.H.H.; Kia, S. Effect of alloy types on the anodizing process of aluminium. *Surf. Coat. Technol.* **2006**, *200*, 2634–2641. [[CrossRef](#)]
77. Zhu, B.; Seifeddine, S.; Persson, P.O.; Jarfors, A.E.; Leisner, P.; Zanella, C. A study of formation and growth of the anodised surface layer on cast Al–Si alloys based on different analytical techniques. *Mater. Des.* **2016**, *101*, 254–262. [[CrossRef](#)]
78. Konieczny, J.; Dobrzański, L.A.; Labisz, K.; Duszczak, J. The influence of cast method and anodizing parameters on structure and layer thickness of aluminium alloys. *J. Mater. Process. Technol.* **2004**, *157*, 718–723. [[CrossRef](#)]
79. Benea, L.; Simionescu-Bogatu, N.; Chiriac, R. Electrochemically obtained Al<sub>2</sub>O<sub>3</sub> nanoporous layers with increased anticorrosive properties of aluminum alloy. *J. Mater. Res. Technol.* **2022**, *17*, 2636–2647. [[CrossRef](#)]
80. Stepniowski, W.J.; Nowak-Stepniowski, A.; Presz, A.; Czujko, T.; Varin, R.A. The effects of time and temperature on the arrangement of anodic aluminum oxide nanopores. *Mater. Char.* **2014**, *91*, 1–9. [[CrossRef](#)]
81. Cabral-Miramontes, J.A.; Bastidas, D.M.; Baltazar, M.A.; Zambrano-Robledo, P.; Bastidas, J.M.; Almeraya-Calderón, F.M.; Gaona-Tiburcio, C. Corrosion behavior of Zn–TiO<sub>2</sub>, and Zn–ZnO Electrodeposited Coating in 3.5% NaCl Solution. *Int. J. Electrochem. Sci.* **2019**, *14*, 4226–4239. [[CrossRef](#)]
82. Samaniego-Gómez, P.; Almeraya-Calderón, F.; Martín, U.; Ress, J.; Gaona-Tiburcio, C.; Silva-Vidaurre, L.; Cabral-Miramontes, J.; Bastidas, J.M.; Chacón-Nava, J.G.; Bastidas, D.M. Efecto del tratamiento de sellado en el comportamiento frente a corrosión de la aleación anodizada de aluminio-litio AA2099. *Rev. Met.* **2020**, *56*, e180. [[CrossRef](#)]
83. Samaniego-Gómez, P.O.; Almeraya-Calderon, F.; Maldonado-Bandala, E.; Cabral-Miramontes, J.; Nieves-Mendoza, D.; Olguin-Coca, J.; Lopez-Leon, L.D.; Silva Vidaurri, L.G.; Zambrano-Robledo, P.; Gaona-Tiburcio, C. Corrosion Behavior of AA2055 Aluminum-Lithium Alloys Anodized in the Presence of Sulfuric Acid Solution. *Coatings* **2021**, *11*, 1278. [[CrossRef](#)]
84. Montoya-Rangel, M.; de Oca, N.G.M.; Gaona-Tiburcio, C.; Colás, R.; Cabral-Miramontes, J.; Nieves-Mendoza, D.; Maldonado-Bandala, E.; Chacón-Nava, J.; Almeraya-Calderón, F. Electrochemical Noise Measurements of Advanced High-Strength Steels in Different Solutions. *Metals* **2020**, *10*, 1232. [[CrossRef](#)]
85. Jaquez-Muñoz, J.M.; Gaona-Tiburcio, C.; Chacón-Nava, J.; Cabral-Miramontes, J.; Nieves-Mendoza, D.; Maldonado-Bandala, E.M.; Delgado, A.D.; Flores-De Los Rios, J.P.; Bocchetta, P.; Almeraya-Calderón, F. Electrochemical Corrosion of Titanium and Titanium Alloys Anodized in H<sub>2</sub>SO<sub>4</sub> and H<sub>3</sub>PO<sub>4</sub> Solutions. *Coatings* **2022**, *12*, 325. [[CrossRef](#)]
86. Chu, S.Z.; Wada, K.; Inoue, S.; Isogai, M.; Yasumori, A. Fabrication of ideally ordered nanoporous alumina films and integrated alumina nanotubule arrays by high-field anodization. *Adv. Mater.* **2005**, *17*, 2115–2119. [[CrossRef](#)]



87. Schwirn, K.; Lee, W.; Hillebrand, R.; Steinhart, M.; Nielsch, K.; Gösele, U. Self-ordered anodic aluminum oxide formed by H<sub>2</sub>SO<sub>4</sub> hard anodization. *ACS Nano* **2008**, *2*, 302–310. [[CrossRef](#)]
88. Noh, K.; Brammer, K.; Kim, H.; Jung, S.; Seong, T.; Jin, S. Highly self-assembled nanotubular aluminum oxide by hard anodization. *J. Mater. Res.* **2011**, *26*, 186–193. [[CrossRef](#)]
89. MIL-A-8625F; Anodic Coatings for Aluminum and Aluminum Alloys. Departments and Agencies of the Department of Defense: The Pentagon Arlington, VA, USA, 1993; pp. 1–19.
90. Lerner, L.M. Hard anodizing of aerospace aluminium alloys. *Trans. Inst. Met. Finish.* **2010**, *88*, 21–24. [[CrossRef](#)]
91. Mansouri, K.; Ibrik, K.; Bensalah, N.; Abdel-Wahab, A. Anodic dissolution of pure aluminum during electrocoagulation process: Influence of supporting electrolyte, initial pH and current density. *Ind. Eng. Chem. Res.* **2011**, *50*, 13362–13372. [[CrossRef](#)]
92. Martínez-Ramos, C.; Olguin-Coca, J.; Lopez-Leon, L.D.; Gaona-Tiburcio, C.; Lara-Banda, M.; Maldonado-Bandala, E.; Castañeda-Robles, I.; Jaquez-Muñoz, J.M.; Cabral-Miramontes, J.; Nieves-Mendoza, D.; et al. Electrochemical Noise Analysis Using Experimental Chaos Theory, Power Spectral Density and Hilbert–Huang Transform in Anodized Aluminum Alloys in Tartaric–Phosphoric–Sulfuric Acid Solutions. *Metals* **2023**, *13*, 1850. [[CrossRef](#)]
93. Zhao, J.; Xu, D.; Shahzad, M.B.; Kang, Q.; Sun, Y.; Sun, Z.; Zhang, S.; Ren, L.; Yang, C.; Yang, K. Effect of surface passivation on corrosion resistance and antibacterial properties of Cu-bearing 316L stainless steel. *Appl. Surf. Sci.* **2016**, *386*, 371–380. [[CrossRef](#)]
94. Esmailzadeh, S.; Aliofkhaezai, M.; Sarlak, H. Interpretation of Cyclic Potentiodynamic Polarization Test Results for Study of Corrosion Behavior of Metals: A Review. *Prot. Met. Phys. Chem. Surf.* **2018**, *54*, 976–989. [[CrossRef](#)]
95. Feliu, S.J. Electrochemical impedance spectroscopy for the measurement of the corrosion rate of magnesium alloys: Brief review and challenges. *Metals* **2020**, *10*, 775. [[CrossRef](#)]
96. Villegas-Tovar, J.; Gaona-Tiburcio, C.; Lara-Banda, M.; Maldonado-Bandala, E.; Baltazar-Zamora, M.A.; Cabral-Miramontes, J.; Nieves-Mendoza, D.; Olguin-Coca, J.; Estupiñan-Lopez, F.; Almeraya-Calderón, F. Electrochemical Corrosion Behavior of Passivated Precipitation Hardening Stainless Steels for Aerospace Applications. *Metals* **2023**, *13*, 835. [[CrossRef](#)]
97. Jáquez-Muñoz, J.M.; Gaona-Tiburcio, C.; Méndez-Ramírez, C.T.; Baltazar-Zamora, M.Á.; Estupiñán-López, F.; Bautista-Margulis, R.G.; Cuevas-Rodríguez, J.; Flores-De los Rios, J.P.; Almeraya-Calderón, F. Corrosion of Titanium Alloys Anodized Using Electrochemical Techniques. *Metals* **2023**, *13*, 476. [[CrossRef](#)]
98. Dzhurinskiy, D.V.; Dautov, S.S.; Shornikov, P.G.; Akhatov, I.S. Surface Modification of Aluminum 6061-O Alloy by Plasma Electrolytic Oxidation to Improve Corrosion Resistance Properties. *Coatings* **2021**, *11*, 4. [[CrossRef](#)]
99. Hoar, T.P.; Wood, G.C. The sealing of porous anodic oxide films on aluminium. *Electrochim. Acta* **1962**, *7*, 333–353. [[CrossRef](#)]
100. Duarte, T.; Meyer, Y.A.; Osório, W.R. The Holes of Zn Phosphate and Hot Dip Galvanizing on Electrochemical Behaviors of Multicoatings on Steel Substrates. *Metals* **2022**, *12*, 863. [[CrossRef](#)]
101. Kramer, G.R.; Mendez, C.M.; Ares, A.E. Evaluation of corrosion resistance of aluminum-based alloys in bioethanol produced in Misiones. *Proc. Mat. Sci.* **2015**, *9*, 341–349. [[CrossRef](#)]
102. Meyer, Y.A.; Menezes, I.; Bonatti, R.S.; Bortolozzo, A.D.; Osório, W.R. EIS investigation of the corrosion behavior of steel bars embedded into modified concretes with eggshell contentes. *Metals* **2022**, *12*, 417. [[CrossRef](#)]
103. Fabris, R.; Masi, G.; Bignozzi, M.C. Corrosion Behavior of Aluminum Alloys in Different Alkaline Environments: Effect of Alloying Elements and Anodization Treatments. *Coatings* **2024**, *14*, 240. [[CrossRef](#)]
104. Mopon, M.L., Jr.; Garcia, J.S.; Manguerra, D.M.; Narisma, C.J.C. Corrosion Behavior of AA 1100 Anodized in Gallic-Sulfuric Acid Solution. *Coatings* **2021**, *11*, 405. [[CrossRef](#)]
105. Elkilany, H.A.; Shoeb, M.A.; Abdel-Salam, O.E. Influence of hard anodizing on the mechanical and corrosion properties of different aluminum alloys. *Metallogr. Microstruct. Anal.* **2019**, *8*, 861–879. [[CrossRef](#)]
106. Habazaki, H.; Shimizu, K.; Paez, M.A.; Skeldon, P.; Thompson, G.E.; Wood, G.C.; Xhou, X. Oxidation of copper and mobility of copper ions during anodizing of an Al–1.5 wt.% Cu alloy. *Surf. Interface Anal.* **1995**, *23*, 892–898. [[CrossRef](#)]
107. Tang, C.W. The Study of Anodic Treatment of Aluminum in Tertiary Mixed Acid after High Temperature Pre-Immersing. Ph.D. Thesis, Tatung University, Taipei City, Taiwan, 2005.
108. Torato, P.; Krusid, B. Effect of current density ramping on the growth rate and structure of AA2024-T3. *Materials* **2022**, *15*, 3258. [[CrossRef](#)] [[PubMed](#)]
109. Zajăczkowska, L.; Siemiaszko, D.; Norek, M. Towards self-organized anodization of aluminum in malic acid solutions—new aspects of anodization in the organic acid. *Materials* **2020**, *13*, 3899. [[CrossRef](#)] [[PubMed](#)]
110. Student, M.; Pohrelyuk, I.; Padgurskas, J.; Rukuiža, R.; Hvozdet's'kyi, V.; Zadorozhna, K.; Veselivska, H.; Student, O.; Tkachuk, O. Abrasive Wear Resistance and Tribological Characteristics of Pulsed Hard Anodized Layers on Aluminum Alloy 1011 in Tribocontact with Steel and Ceramics in Various Lubricants. *Coatings* **2023**, *13*, 1883. [[CrossRef](#)]

**Disclaimer/Publisher's Note:** The statements, opinions and data contained in all publications are solely those of the individual author(s) and contributor(s) and not of MDPI and/or the editor(s). MDPI and/or the editor(s) disclaim responsibility for any injury to people or property resulting from any ideas, methods, instructions or products referred to in the content.